Efforts to localize oscillators driving food-anticipatory behavioral rhythms have for many years relied on lesion experiments, guided by assumptions about likely input–output characteristics of a food-entrainable clock, and more recently by the results of studies in which daily rhythms of clock gene expression have been mapped in the brains of mice and rats anticipating a daily mealtime. Controversy has arisen about the role of the dorsomedial hypothalamic nucleus (DMH) as a putative food-entrainable oscillator 'critical' for food-anticipatory behavioral and temperature rhythms (Davidson, 2006). The DMH is well situated for such a role, given its position within the mediobasal hypothalamic circuits regulating metabolism, feeding and daily sleep–wake cycles (Thompson *et al.*, 1996; Thompson & Swanson, 1998; Bellinger & Bernardis, 2002). In mice, DMH neurons clustered within the pars compacta exhibit circadian cycles of clock gene expression during restricted daytime feeding (Mieda *et al.*, 2006). Rats also exhibit daily rhythms of *Per2* expression in the DMH in association with anticipation of a single daytime meal, although not when anticipating a palatable daily snack (Verwey *et al.*, 2007). In rats, cell-specific lesions of the DMH were reported to significantly, but partially, attenuate or eliminate food-anticipatory rhythms of general activity and body temperature, measured by telemetry (Gooley *et al.*, 2006). However, two subsequent studies have failed to detect an effect of complete radiofrequency DMH lesions on food-anticipatory activity rhythms in rats, measured by general or area-specific motion sensors (Landry *et al.*, 2006, 2007). It has been suggested that motion sensors and telemetry may be differentially sensitive to non-circadian factors regulating activity (Gooley & Saper, 2007), but concurrent measurements from the same animals indicate that, in rats, these methods produce virtually identical results (Mistlberger *et al.*, 2009a). At present, the conflicting results from rat lesion studies have not been reconciled (Landry & Mistlberger, 2007).

Additional evidence that the DMH is the site of circadian oscillators driving food-anticipatory activity comes from a recent study claiming that food-anticipatory rhythms are absent in mice with a null mutation of the clock gene *BMAL1* and are rescued in *BMAL1*−/− mice in which *BMAL1* expression is selectively restored in the DMH by adeno-associated viral vector (Fuller *et al.*, 2008). However, it has also been reported that *BMAL1*−/− mice exhibited robust food-anticipatory rhythms (Mistlberger *et al.*, 2008; Pendergast *et al.*, 2009; Storch & Weitz, 2009), and the evidence as presented in Fuller *et al.* has significant short comings (Mistlberger *et al.*, 2009b). So far, there are no studies of food-anticipatory rhythms in mice with DMH lesions.

The present study seeks to fill several important knowledge gaps toward clarifying the role of putative DMH circadian oscillators in behavioral, physiological and neural clock gene responses to daily feeding schedules in mice. First, we examined circadian rhythms of clock gene expression (*mBMAL1* and/or *mPer1*, *mPer2*) within the DMH and several other forebrain and brainstem regions during fasting, after one midday meal, and after a week or more of midday-restricted feeding. We then probed the neurochemical basis for clock gene responses within the DMH by treating mice with a glutamate antagonist prior to a single midday feeding or after a week of midday feedings. Finally, we used thermal lesions to determine whether the DMH is critical for feeding-induced clock gene expression elsewhere in the brain, and for food-anticipatory rhythms of activity and core temperature. The results confirm that clock genes in DMH cells are rapidly induced by a single feeding and exhibit a daily rhythm of expression that is set by mealtime and persists during food deprivation. However, the results further show that acute clock gene induction and food-entrained rhythms of behavior, temperature and clock gene expression in brainstem and forebrain areas are virtually unaffected by DMH ablation.

Materials and methods

Animals

Six-week-old male ddY mice (Takasugi Animal, Tokyo, Japan) were entrained to a 12:12 h LD cycle in temperature-controlled animal quarters (23 ± 2°C). All mice were housed in polypropylene cages with wood shavings. Food and water were provided *ad libitum*. All experiments were approved by the Experimental Animal Welfare Committee in the School of Human Sciences of Waseda University (Permission #00-17), and conducted according to the Law (No.105) and Notification (No.6) of the Japanese Government.

Restricted feeding schedules for clock gene expression in intact mice

To examine the acute effect of daytime feeding on *mPer1* and *mPer2* mRNA levels in selected brain regions, mice were fed either *ad libitum* or were food-deprived for 18 h, from Zeitgeber time (ZT) 11 (1 h before lights-off, which is designated ZT12 by convention) to ZT5 the following day. Food was then provided for up to 4 h, and groups of mice (*n* = 3–5) were decapitated at ZT6, 7, 9 or 12 (1, 2, 4 or 7 h after food was reintroduced, respectively).

To examine the effects of restricted daytime feeding on *mPer1*, *mPer2* and *mBMAL1* mRNA expression across the 24-h day, mice were assigned to one of four experimental conditions: (i) *ad libitum* food access; (ii) food deprivation from ZT11; (iii) food deprivation from ZT11 and a single feeding from ZT5 to ZT9; and (iv) food deprivation from ZT11 and a daily ZT5–ZT9 feeding for six consecutive days. Mice in the first three conditions were killed in groups of two–seven at 4-h intervals, from ZT19 to ZT15 the next day, i.e. spanning one full 24-h day either with food available, with no food, or with no food after a single ZT5–ZT9 feeding, respectively. Mice in condition four were killed in groups of three–seven from ZT19 to ZT15 2 days later, i.e. spanning two full 24-h cycles with no food after six consecutive days of ZT5–ZT9 feeding.

To examine mPER2 protein expression in the DMH, an additional three groups of mice (*n* = 5–8) were killed at ZT4–ZT6, ZT10–ZT12 or ZT14–ZT16 after 6 days of restricted feeding from ZT5 to ZT9.

Glutamate antagonist and clock gene expression in the DMH

The emergence of food-anticipatory behavioral rhythms in rats can be attenuated by daily treatment with the glutamate antagonist +MK801 (Ono *et al.*, 1996). The DMH receives glutamatergic input from circumventricular organs, such as the organum vasculosum laminae terminalis and the subfornical organ (Richard & Bourque, 1992; Grob *et al.*, 2003; Johnson & Shekhar, 2006), and *N*-methyl-D-aspartate (NMDA) receptors in the DMH are involved in mediating the autonomic cardiovascular response to appetitive feeding (De Matteo *et al.*, 2006). If the DMH is the site of action for effects of MK801 on food-anticipatory rhythms, then +MK801 may be expected to also block effects of feeding on DMH clock gene expression. To examine the effects of +MK801 on induction of *mPer1* and *mPer2* by a single ZT5 meal, mice food-deprived from ZT11 received an i.p. injection of +MK801 (Research Biochemicals, Natick, MA, USA; 0.0, 0.1 or 0.5 mg/kg in saline) at ZT4.5, were fed at ZT5 and killed at ZT7. To examine the effects of +MK801 on the endogenous rhythm of *mPer1* and *mPer2* expression induced by repeated midday feedings, mice were food-deprived at ZT11, fed from ZT5 to ZT9 for six consecutive days, received an i.p. injection of +MK801 (0 or 0.5 mg/kg) at ZT0, and were killed at ZT7 without

feeding. The drug injections were timed to precede by ~3 h the rise of *mPer1* and *mPer2* expression that was observed in the experiments described above.

DMH lesions and feeding schedules for behavior, temperature and clock gene measurements

Mice were anesthetized with ketamine (50 mg/kg i.p.) and hydrazine (20 mg/kg i.p.), and positioned in a stereotaxic frame (Narishige, Tokyo, Japan) for placement of stainless steel electrodes (0.35 mm diameter) into the DMH. Stereotaxic coordinates were 1.9 mm posterior and ± 0.3 mm lateral to bregma and 6.2 mm below the skull surface. Bilateral lesions were made with a thermal lesion device (RFG-4A, Muromachi, Tokyo, Japan) that heated the electrode tip to 55°C for 3 s via a current path. Sham-operated mice were treated in the same manner, but without the current path. Seven days after the operation, subsets of control and DMH-lesion mice were anesthetized and laparotomized to implant temperature loggers (3650, HIOKI, Nagano, Japan) in the peritoneal cavity. All mice were given 10–21 days to recover from surgery in LD with food access *ad libitum*.

To assess the effect of DMH ablation on acute affects of feeding on clock genes outside of the DMH, groups ($n = 5$–7) of sham and DMH-lesion mice were fed *ad libitum* or were food-deprived from ZT11 to ZT5, fed for 2 h and then killed at ZT7 for *in situ* hybridization of *mPer1* and *mPer2* mRNA.

To assess the effect of DMH ablation on locomotor activity and clock gene responses to a daily feeding schedule in LD conditions, groups of sham and DMH-lesion mice were housed individually in transparent plastic cages (31 × 20 × 13 cm). Activity was measured by infrared motion sensors (Omron F5B, Kyoto, Japan) positioned over the food hopper (16 cm width × 4.5 cm depth × 9 cm height) located along the narrow side of the animal cage. Because the infrared motion sensors were positioned approximately 2 cm above the cage top at the center of the food hopper, we monitored the animal movement within the semicircle area (88 cm^2 at the level of animal location, which is calculated to about 14% of the total area of the animal cage floor) including the hopper place. This enables us to take indirect and relative measurements of the food-access behavior in mice. Mice were food-deprived starting at ZT11, fed from ZT5 to ZT9 for 6 days (Day 1–Day 6), food-deprived for 1 day (Day 7), fed from ZT5 to ZT9 for another 6 days (Day 8–Day 13), and food-deprived until being killed on Day 15 as described below. On the last day of food deprivation (Day 15, i.e. the 15th day after the beginning of the restricted feeding), mice were killed at either ZT7 or ZT19 for *in situ* hybridization. Thus, the duration of the last food deprivation after the end of the last meal was 46 h or 58 h in mice sampled at ZT7 or ZT19, respectively.

To assess the effect of DMH ablation on food-anticipatory rhythms of locomotor activity and core body temperature in constant dark (DD), sham and DMH-lesion mice with i.p. temperature loggers were housed in the same plastic cages, and subjected to the same feeding schedule as in the locomotor activity and clock gene experiments in LD. Daily feedings were again omitted on Days 7, 14 and 15, but the lights were left off on those days to determine if food-anticipatory rhythms were cued by LD. These mice were not used for *in situ* hybridization.

Verification of DMH lesions

Serial coronal sections (30 μm) from sham and DMH-lesion mice were stained with Cresyl violet and photographed through the DMH area using a digital camera attached to a light microscope. The borders of the DMH were drawn on the digital images and the area of the DMH was calculated using SCION IMAGE software (SCION, MD, USA). The proportion of the DMH that was ablated was estimated as [100 − (the area of remaining DMH in an individual lesioned mouse/the averaged area of the DMH of control mice × 100) %].

In situ *hybridization using a radioisotope-labeled cRNA probe*

The details of this procedure have been published previously (Moriya *et al.*, 2000). Briefly, at the appropriate time, mice were deeply anesthetized with ether and intracardially perfused with chilled saline (25 mL) followed by 0.1 M phosphate buffer (pH 7.4) containing 4% paraformaldehyde (25 mL). Coronal slices (30 μm) that included the brain structures of interest were made using a cryostat (HM505E, Microm, Walldorf, Germany). *In situ* hybridization using cRNA probes was used to determine the expression levels of *mPer1*, *mPer2* and *mBMAL1* mRNAs [nucleotide positions: *mPer1* (538–1752); *mPer2* (1–638); *mBMAL1* (1656–2259)]. Slices were divided into four equal sections along the rostro-caudal plane for the measurement of *mPer1*, *mPer2* and *mBMAL1* mRNA levels. mRNAs were visualized by autoradiogram using BioMax MR film (Eastman Kodak, Rochester, NY, USA), and their levels were analysed using an image-analysing system (MCID, GE Healthcare Life Sciences, GE Healthcare UK, Amersham Place, Buckinghamshire, UK) after conversion into optical density by ^{14}C-autoradiographic microscales (GE Healthcare Life Sciences). Optical densities were calculated for the SCN, parietal cortex (CTX), caudate putamen (CP), hypothalamic paraventricular nucleus (PVN), ventromedial hypothalamic nucleus (VMH), DMH, arcuate nucleus (ARC), nucleus of solitary tract (NTS) and area postrema (AP).

Immunohistochemistry

Immunohistochemistry was performed by applying the avidin-biotin-peroxidase method to free-floating sections. Serial coronal sections (30 μm) from the rostral end to the caudal end of the DMH were incubated with anti-mPER2 (1 μg/mL, affinity-purified rabbit anti-sera; Alpha Diagnostic International, San Antonio, TX, USA) and stained brown for visualization with 3,3'-diaminobenzidine tetrahydrochloride (Matsuo *et al.*, 2003). The number of mPER2-positive cells was counted within a fixed area (15 000 μm^2) of the DMH (4 sections/brain).

Data analysis and statistics

Motion sensor counts were summed and stored at 6-min intervals using data acquisition and analysis software of our own design. Activity data were displayed in the form of actograms and average waveforms. For waveforms, activity data were collapsed into 1-h time bins and displayed as counts relative to the daily total, i.e. counts for each hour as a percentage of total daily counts for the day. Core body temperature was continuously monitored, averaged in 15-min time bins and analysed using the manufacturer's software. Values in the text and figures are expressed as means ± SEM. For *in situ* hybridization data, we performed the statistical analysis using the raw data. For statistical analysis, an unpaired Student's *t*-test or one-way ANOVA followed by the Tukey–Kramer test were used. The significance level in all analyses was 0.05.

Results

A single midday meal induces mPer1 *and 2 expression in the DMH, ARC, NTS and AP*

We first examined the effect of a single feeding from ZT5 to ZT9, following an overnight fast, on *mPer1* and *mPer2* mRNA in selected areas of the forebrain and brainstem. The DMH, ARC, NTS and AP all exhibited significant elevations of *mPer1* and/or *mPer2* at 1, 2, 4 and/or 7 h after meal onset (Fig. 1, Supplemental Fig. S1). The SCN, CTX, CP, PVN and VMH did not show a significant acute effect of feeding; expression levels at the 2-h time point (ZT7) for these structures are presented in Table 1. Among the areas quantified, the DMH exhibited by far the largest increases of gene expression (Fig. 1B and C, Supplemental Fig. S1). *mPer1* and *mPer2* mRNAs were increased throughout the DMH, but most prominently within the pars compacta of the caudal DMH (Fig. 1B). The levels of *mPer1* mRNA in the DMH were significantly elevated 1 h after the onset of feeding, and were highest 2 h after feeding. By 7 h after feeding (ZT12), expression decreased to basal levels similar to those in control mice. *mPer2* mRNA in the DMH was also increased 1 h after meal onset, but increased further at the 2-h and 4-h time points, and although declining was still significantly elevated at ZT12 [Control, 138.3 ± 5.7 ($n = 3$); Re-fed, 121.0 ± 0.4 ($n = 3$), $P < 0.05$]. In the ARC, NTS and AP, *mPer1* and *mPer2* mRNA levels were increased only at the 1-h and/or 2-h time points (Fig. 1C).

Scheduled midday feeding shifts the daily rhythm of clock gene expression in the DMH, ARC and CTX

We next examined the daily profiles of *mPer1*, *mPer2* and *mBMAL1* expression in the DMH, ARC, CTX and SCN of mice during *ad libitum* food access or during 1 or 2 days of fasting after either *ad libitum* food access, one midday (ZT5–ZT9) feeding or six consecutive midday feedings. The ARC and CTX were selected to represent regions that differed in the response of *mPer1* and *mPer2* to a single feeding. The SCN was included as a positive control, given its known circadian profile and known minimal resetting response to restricted feeding in LD (e.g. Damiola *et al.*, 2000; Stokkan *et al.*, 2001).

In the DMH, daily rhythms of *mPer1*, *mPer2* and *mBMAL1* mRNA expression were observed in control mice fed *ad libitum* ($P < 0.05$, one-way ANOVA; Fig. 2, Supplemental Fig. S2). *mPer1* and *mPer2* expression peaked around dusk or early nighttime, while *mBMAL1* expression peaked during the day (ZT3). This daily rhythm of *mPer1* mRNA expression in the DMH under *ad libitum* feeding condition is similar to that reported previously, which described a ~three–fourfold higher expression near the onset of the dark phase (ZT13) compared with the mid-light phase (ZT7; Mieda *et al.*, 2006). Fasting after *ad libitum* food access had no effect on the timing or amplitude of these rhythms. However, a single daytime feeding from ZT5 to ZT9, after an 18-h fast, was associated with a marked (4–12 h) shift in the timing of peak expression and an increase in the amplitude of the daily rhythm of all three clock genes, assessed during a fasting day after the meal. Phase and amplitude changes of the same magnitude and direction were apparent across 2 days of fasting after six consecutive midday feedings.

Comparable feeding-induced changes in phase and amplitude of *mPer1*, *mPer2* and *mBMAL1* mRNA rhythms were also evident in the ARC and CTX following one or six consecutive ZT5–ZT9 feedings (Supplemental Figs S2–S4). By contrast, the SCN exhibited high-amplitude daily rhythms of clock gene expression that were unaltered by restricted daytime feeding (Supplemental Fig. S5).
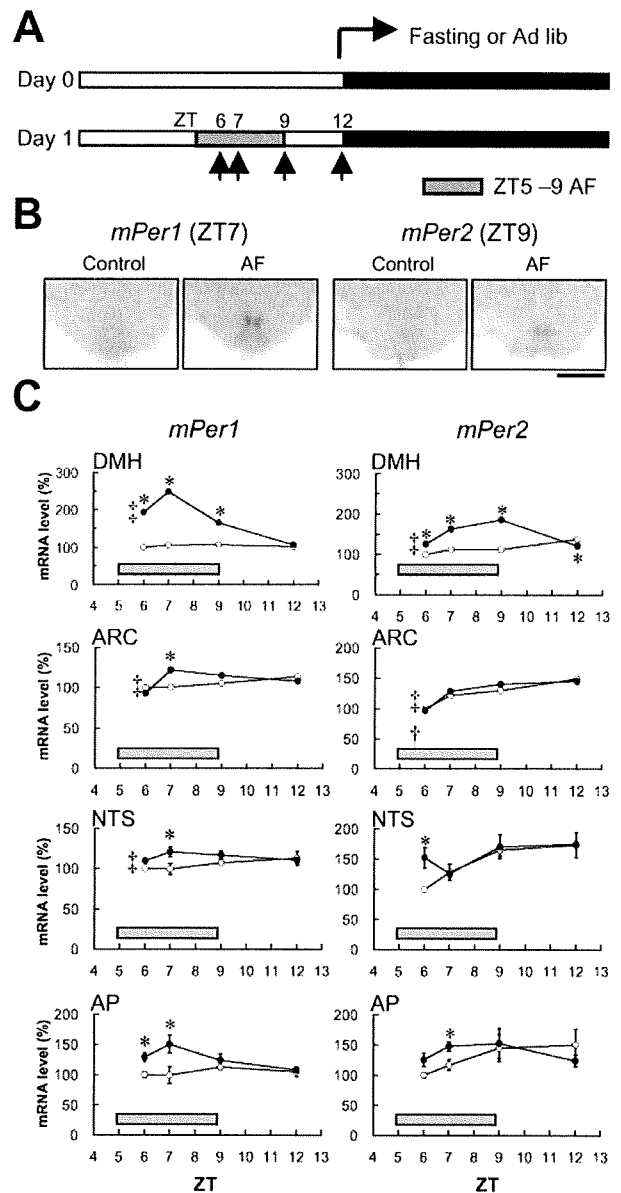

FIG. 1. *mPer1* and *mPer2* mRNA expression induced by midday feeding after an overnight fast. (A) Sampling schedules. The open, closed and gray bars indicate the light, dark and feeding periods, respectively. The upward arrows show the time of death. (B) Representative autoradiograms demonstrating the effect of feeding on the levels of *mPer1* and *mPer2* mRNAs in the dorsomedial hypothalamic nucleus (DMH) at ZT7 and ZT9, respectively. The scale bar indicates 1.0 mm. (C) Time-course of feeding-induced changes in *mPer1* and *mPer2* mRNA levels in the DMH, arcuate nucleus (ARC), nucleus of the solitary tract (NTS) and area postrema (AP). The open and closed circles indicate *ad libitum* fed control ($n = 3$–5) and re-fed mice ($n = 3$–5), respectively. The values at Zeitgeber time (ZT)6 for control mice are set to 100%. The horizontal gray boxes indicate the feeding time. Note that the scales of the vertical axes are different among graphs. $^{\dagger}P < 0.05$ for the effect of ZT in the control group (one-way ANOVA). $^{\ddagger}P < 0.05$ for the effect of ZT in the acute feeding (AF) group (one-way ANOVA). $*P < 0.05$ vs. control group (Tukey–Kramer's test).

PER2 protein expression in the DMH exhibits a daily rhythm in rats under daytime restricted-feeding conditions (Verwey *et al.*, 2007). We therefore examined the expression of mPER2 immunoreactivity in the DMH of mice during a fasting day following 6 days of restricted

TABLE 1. Acute effects of feeding on *mPer1* and *mPer2* mRNA levels in various areas of the brain

Brain area	Control (C) (nCi/g)	Acute feeding (AF) (nCi/g)	Ratio (AF/C)
mPer1			
SCN	204.7 ± 19.0	195.2 ± 8.5	0.953
Cortex	113.0 ± 9.9	139.8 ± 13.0	1.237
CP	75.4 ± 6.3	87.3 ± 8.4	1.158
PVN	88.9 ± 5.3	91.7 ± 9.1	1.032
VMH	103.4 ± 10.7	104.9 ± 11.1	1.015
mPer2			
SCN	465.9 ± 16.2	503.8 ± 19.5	1.081
Cortex	131.0 ± 14.7	161.8 ± 19.4	1.235
CP	128.5 ± 8.5	141.9 ± 15.1	1.104
PVN	87.4 ± 8.7	95.6 ± 4.8	1.094
VMH	118.5 ± 8.4	112.3 ± 9.8	0.948

After overnight fasting, mice (AF group, n = 4–5) were given food from ZT5 and decapitated at ZT7 (2 h after the onset of feeding). Control mice (n = 4–5) were allowed access to food *ad libitum* and then decapitated at ZT7. *mPer1* and *mPer2* mRNA levels were measured by *in situ* hybridization methods. CP, caudate putamen; PVN, hypothalamic paraventricular nucleus; SCN, suprachiasmatic nucleus; VMH, ventromedial hypothalamic nucleus.

feeding. In *ad libitum* fed control mice, there was a sparse number of mPER2-positive cells in the DMH at three time points (ZT4–ZT6, ZT10–ZT12 and ZT14–ZT16). In mice on restricted daytime feeding, the number of mPER2-positive cells on the fasting day was also low at ZT4–ZT6, but significantly and progressively increased at the two later time points (Supplemental Fig. S6). Similar to results in rats (Verwey *et al.*, 2007), mPER2-positive cells were limited to the pars compacta, which in mice is within 200 μm lateral to the third ventricle.

+MK801 blocks feeding-induced but not feeding-entrained expression of mPer1 and mPer2 in the DMH

+MK801 administered at ZT4.5 dose-dependently blocked *mPer1* and *mPer2* expression in the DMH, assessed at ZT7 following meal onset at ZT5 (Fig. 3). To examine the effect of +MK801 on feeding-entrained expression of *mPer1* and *mPer2* in the DMH, we administered the drug at ZT0 and subsequently sampled the brains at ZT7, as the circadian rise either in *mPer1* or *mPer2* mRNA in the DMH of food-entrained rats was observed especially between ZT0 and ZT7 (Fig. 2D). However, +MK801 administered at ZT0 did not affect the ZT7 peak of *mPer1* and *mPer2* expression in the DMH of mice on a fasting day after six consecutive days of ZT5–ZT9 feeding (Fig. 4). The drug did not affect meal size at any dose.

DMH lesion histology

Photomicrographs of the DMH area in representative sham and lesion mice are shown in Fig. 5. In 28 out of 46 mice, the DMH lesions were judged to be > 80% complete, and only these mice were included in clock gene and behavioral analyses. In these cases, lesion cavities extended ~500 μm lateral from the third ventricle, and appeared to bilaterally destroy the pars compacta, the DMH region in which both *mPer* mRNA and mPER2 protein were expressed in intact mice. In most brains, some DMH on one or both sides was spared laterally in its most ventral aspect. Collateral damage in brains with the largest lesions was apparent ventrally in the most dorsal aspect of the VMH, dorsally in the midline thalamus (the reunions and rhomboid nuclei,

e.g. #32, #33, #34 in Fig. 5) and caudally in the mammillary nucleus (e.g. #22, #27, #32, #34, #42, #43, #45 in Supplemental Fig. S7).

DMH lesion effects on food intake and body weight

Food intake and body weight data were collected from a subset of sham and DMH-lesion mice that were used for *in situ* hybridization but not for behavioral or temperature recordings. Relative to sham lesion mice, DMH-lesion mice showed a small but significant increase of daily food intake under *ad libitum* feeding conditions [food intake (g/day), Sham: 5.1 ± 0.19 g (n = 10), DMH-lesion: 5.9 ± 0.21 g (n = 13), $P < 0.05$ (Student's *t*-test)] and a small but significant decrease of food intake from ZT5 to ZT9 after overnight fasting [food intake (g/2 h), Sham: 2.2 ± 0.19 g (n = 6), DMH-lesion: 1.4 ± 0.14 g (n = 6), $P < 0.01$ (Student's *t*-test)]. However, by the second week of restricted daytime feeding, 4-h food intake was the same in sham and DMH-lesion mice [food intake (g/4 h), Sham: 3.9 ± 0.29 g (n = 6), DMH-lesion: 3.7 ± 0.26 g (n = 6), $P > 0.05$ (Student's *t*-test)]. Body weight was transiently decreased in DMH-lesion mice but recovered within 10 days after surgery (data not shown), and body weights did not differ between sham and DMH-lesion groups, either immediately before or after restricted daytime feeding.

DMH lesions do not affect acute feeding-evoked or feeding-entrained expression of mPer1 or mPer2 in other brain regions

To determine whether the DMH is necessary for the acute effect of feeding on clock gene expression in the ARC, NTS and AP, *mPer1* and *mPer2* expression were quantified in these structures in mice with DMH lesions. As shown in Fig. 6B, DMH lesions had no effect on *mPer1* or *mPer2* expression in these areas, measured at ZT7 following meal onset at ZT5 after an overnight fast.

We next examined whether the DMH is necessary for the daily variation of *mPer2* expression evident in the ARC and CTX on Day 15 of the restricted daily (ZT5–ZT9) feeding schedule. In both structures, *mPer2* expression was significantly elevated at ZT7 relative to ZT19 on a fasting day after the last day of restricted feeding, and there were no differences between sham and DMH lesion groups (Fig. 7). *mPer2* mRNA was also quantified in the SCN, and while there was no difference between groups in expression levels at ZT19, expression levels at ZT7 were significantly higher in DMH-lesion mice than in the sham lesion mice (Fig. 7).

DMH lesions do not affect food-anticipatory activity or temperature rhythms in LD or DD

Relative to sham lesion mice, DMH-lesion mice exhibited a marked reduction of total daily locomotor activity during *ad libitum* food access and restricted feeding [total activity count, Sham: 9040 ± 1915 (n = 11), DMH-lesion: 3548 ± 1236 (n = 11), $P < 0.05$ (Student's *t*-test)]. However, when hourly activity counts were expressed as a percentage of total daily activity, the distributions of activity across the day were very similar in sham and DMH-lesion groups (Fig. 8B). During *ad libitum* food access in LD, DMH-lesion mice tended to be less nocturnal than sham mice (Fig. 8A and B) [ratio of nighttime activity to total day activity, Sham: 0.81 ± 0.04 g (n = 11), DMH-lesion: 0.70 ± 0.07 g (n = 11), $P = 0.17$ (Student's *t*-test)], but when food was restricted to ZT5–ZT9 there were no group differences in the magnitude or timing of food-anticipatory activity. Group mean activity waveforms were virtually identical on the two meal omission days, and correlations between lesion size and locomotor anticipation ratios
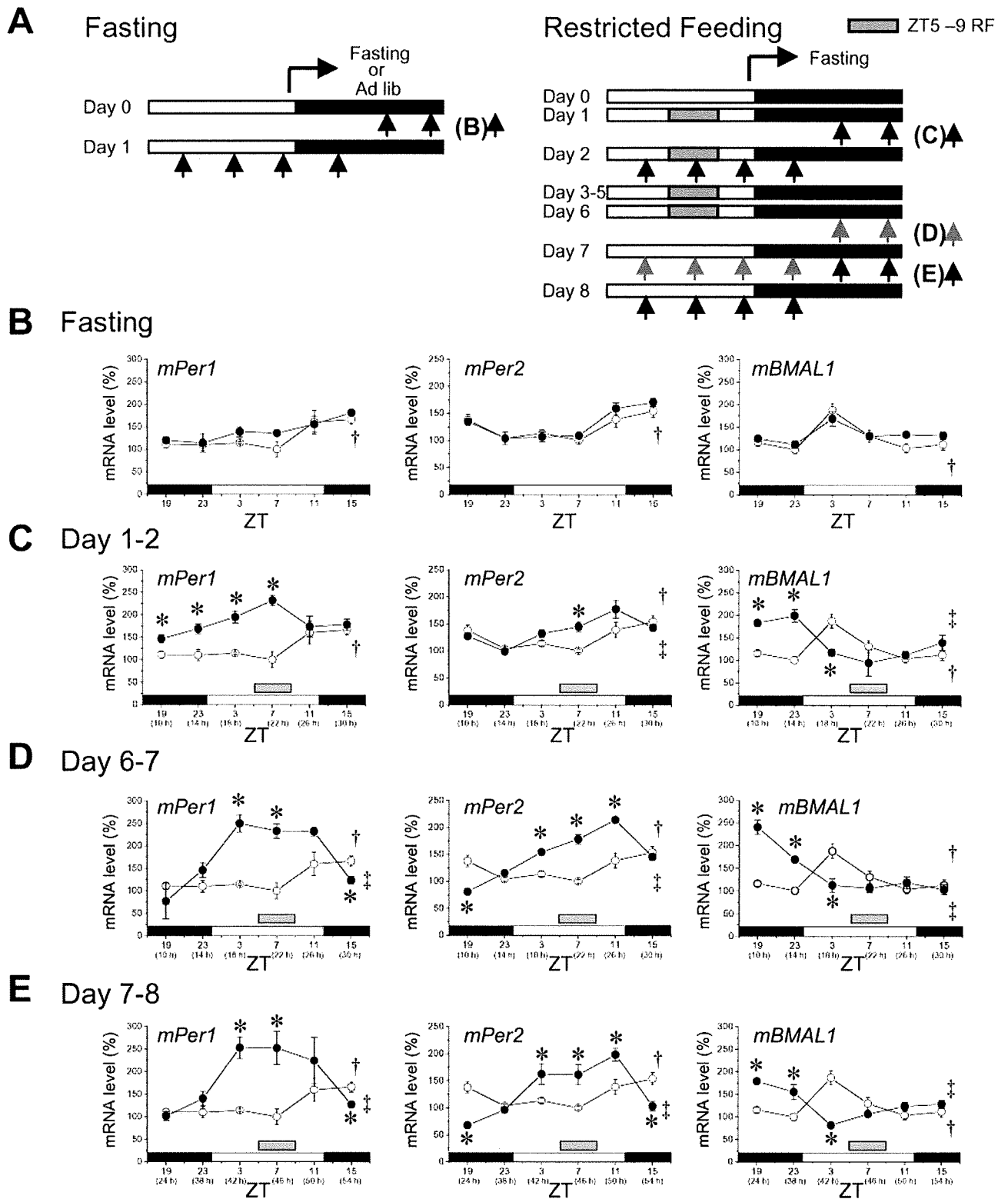
FIG. 2. Expression rhythms of *mPer1*, *mPer2* and *mBMAL1* mRNAs in the DMH of *ad libitum* fed control mice (open circles) and mice fasted with or without refeeding at Zeitgeber time (ZT)5–ZT9 for one or more days (closed circles). (A) Sampling schedules. Horizontal open, closed and gray bars indicate light, dark and feeding periods, respectively. (B) Mice fasted from ZT11. (C) Mice fasted from ZT11 and fed at ZT5–ZT9 for 1 day. Mice fasted from ZT11 and fed at ZT5–ZT9 for 6 days and killed after missing one (D) or (E) two feedings. Horizontal open, closed and gray bars in the bottom of each graph indicate light, dark and previous feeding time, respectively. The numbers in the parentheses on the *x*-axis in (C–E) indicate the sampling time after last meal. The lowest values for control mice are set to 100%, and all other values for control and food-deprived mice are expressed relative to this. Each data point is a mean + SEM of two–seven animals. $^{\dagger}P < 0.05$ for the effect of ZT in the control group (one-way ANOVA). $^{\ddagger}P < 0.05$ for the effect of ZT in the food-restricted group (one-way ANOVA). $*P < 0.05$ vs. control group (Tukey–Kramer's test).

A

Fasting

Day 0

Day 1

ZT 4.5   7

+MK801   Brain sampling

ZT5 −9 AF

B   mPer1

*   *

200
175
150
125
100
75
50
25
0

mRNA level (%)

0   0   0.1   0.5   0.5   +MK801 (mg/kg)

AF

C   mPer2

*   *

200
175
150
125
100
75
50
25
0

mRNA level (%)

0   0   0.1   0.5   0.5   +MK801 (mg/kg)

AF

A

Fasting

Day 0

Day 1-6

ZT 0   7

Day 7

+MK801   Brain sampling   ZT5 −9 RF

B

mPer1

120
100
80
60
40
20
0

mRNA level (%)

Saline   +MK801 (0.5 mg/kg)

C

mPer2

120
100
80
60
40
20
0

mRNA level (%)

Saline   +MK801 (0.5 mg/kg)
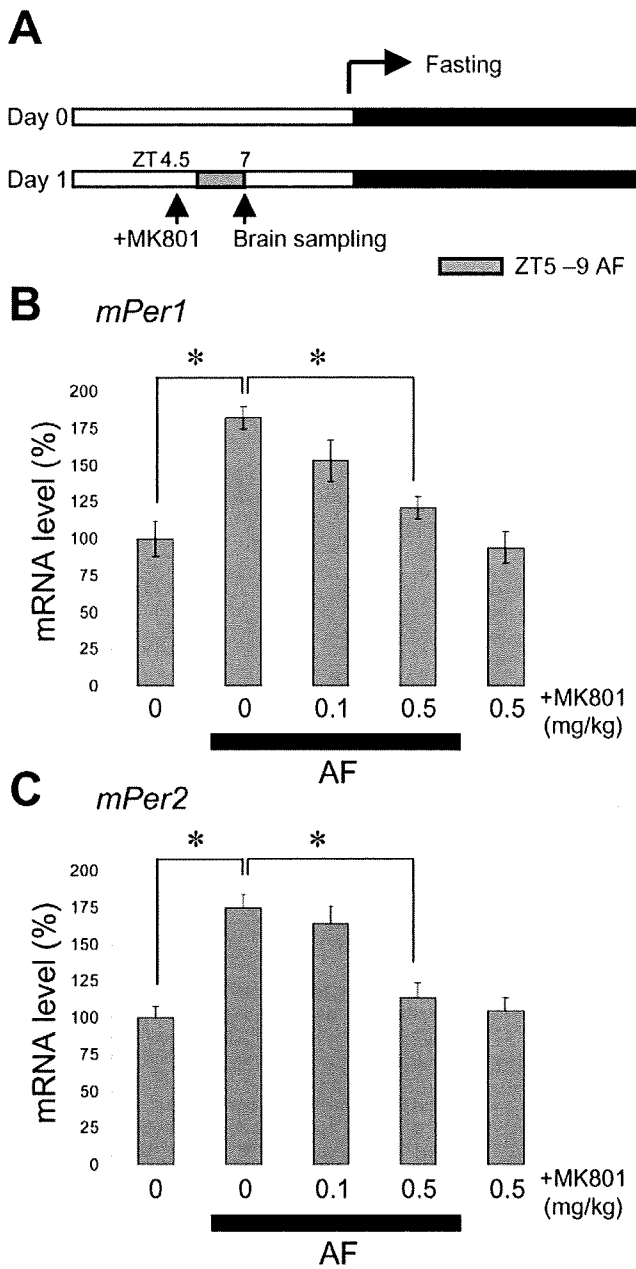
FIG. 3. Effect of NMDA receptor antagonist on acute feeding (AF)-induced mPer1 (B) and mPer2 (C) mRNA expression in the DMH. (A) Sampling schedules. The open, closed and gray bars indicate the light, dark and feeding periods, respectively. After overnight fasting, mice received 0.0, 0.1 or 0.5 mg/kg of +MK801 in saline at Zeitgeber time (ZT)4.5. These mice were then given food from ZT5 to ZT7 and decapitated at ZT7 (2 h after the onset of feeding). Control mice were fed *ad libitum*, received 0.0 or 0.5 mg/kg +MK801 in saline at ZT4.5, and were decapitated at ZT7. The values for control mice in the 0.0 mg/kg group were set to 100%, and all other values are expressed relative to this. *$P < 0.05$ (one-way ANOVA followed by Tukey–Kramer's test). Each group is made up of four animals.

(activity from ZT2 to ZT5 divided by total daily activity) on these days were not significant (Day 7, $R = 0.001$, $P = 0.9985$; lesion size vs. locomotor anticipation on Day 14, $R = 0.161$, $P = 0.7780$).

Similar results were obtained for activity (Fig. 8C) and core body temperature (Fig. 9) measured in additional groups of sham ($n = 5$) and DMH-lesion ($n = 5$) mice bearing intraperitoneal temperature
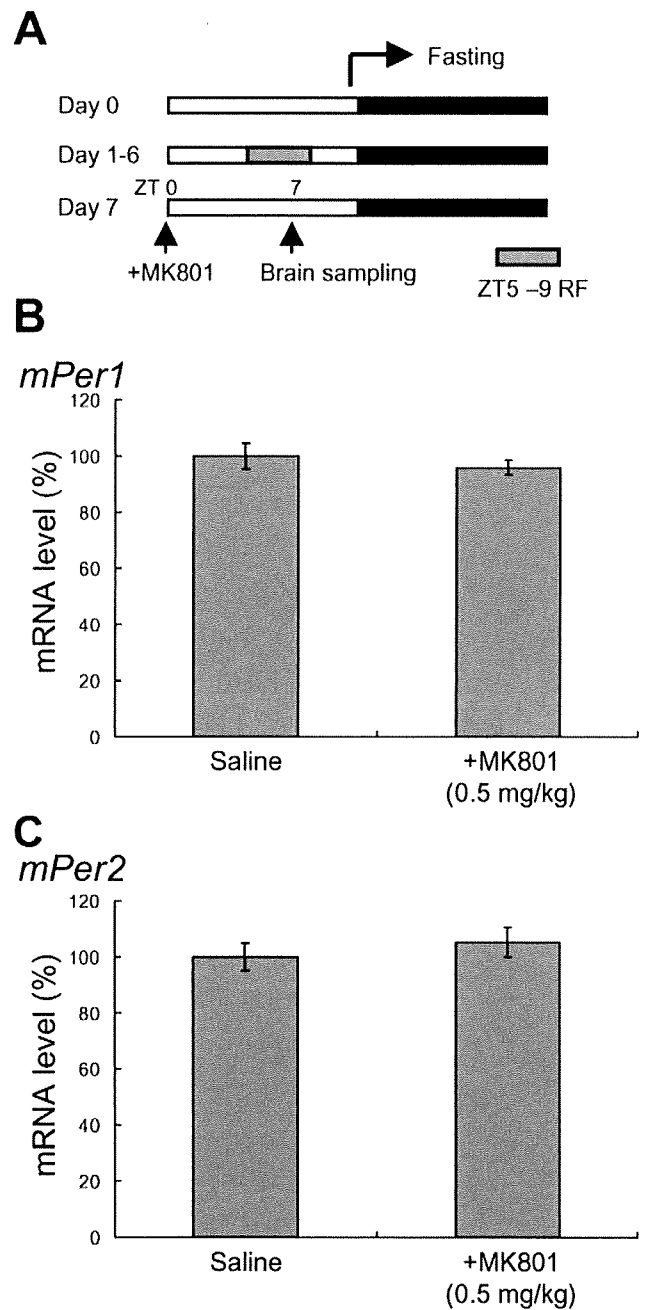
FIG. 4. Effect of NMDA receptor antagonist on mPer1 (B) and mPer2 (C) mRNA expression in the DMH after six consecutive days of restricted daytime feeding. (A) Sampling schedules. See Fig. 3 for plotting conventions. After overnight fasting, mice were allowed to access food from Zeitgeber time (ZT)5 to ZT9 on Days 1–6. On Day 7, mice received +MK801 (0.5 mg/kg) or saline at ZT0, and were decapitated at ZT7 without feeding. The values for *ad libitum* fed control mice were set to 100%. Each group is made up of four animals.

loggers. For these groups, the lights were left off during the meal omission days (Days 7 and 14). DMH lesions modestly attenuated the day–night rhythm of body temperature in LD, but again did not affect the magnitude or timing of the food-anticipatory rise of activity or temperature during daytime-restricted feeding in LD, or during meal omission days in DD. Correlation coefficients relating DMH lesion size with locomotor anticipation and preprandial temperature on the meal omission test days in DD varied from positive to negative and
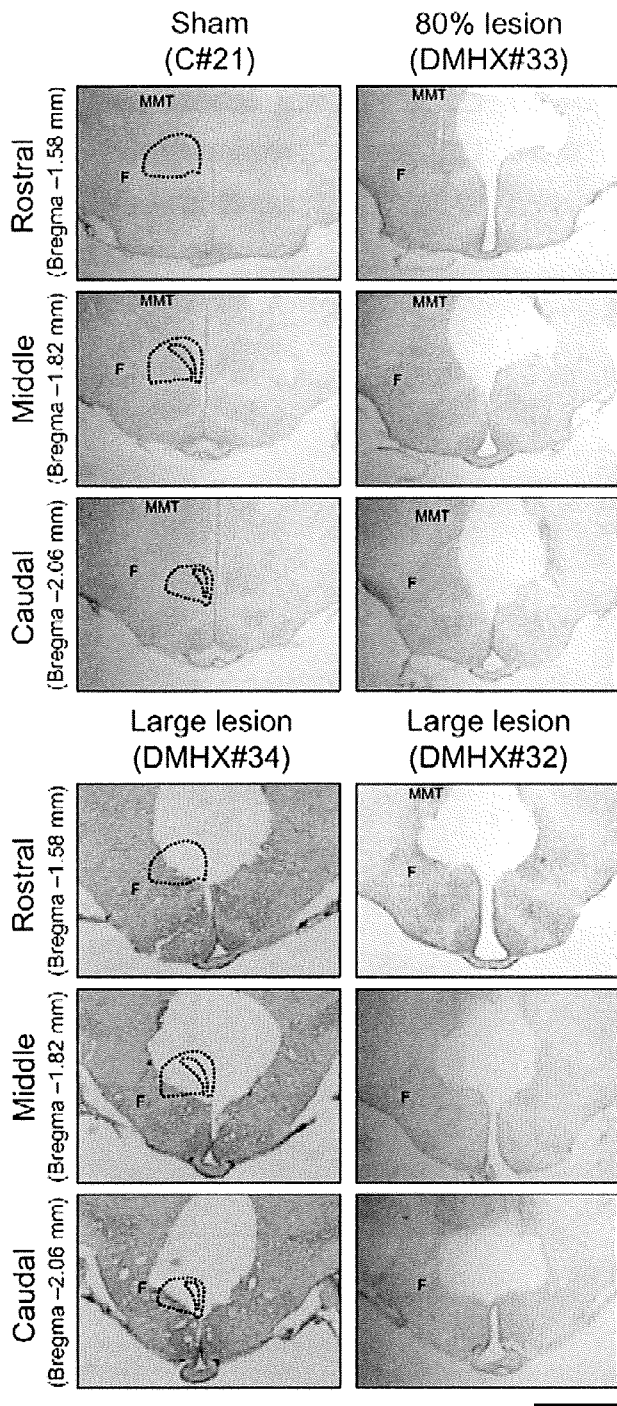
FIG. 5. Representative photomicrographs of Cresyl violet-stained brain sections from mice with sham, 80% or large dorsomedial hypothalamic nucleus (DMH) lesions, at rostral, middle and caudal levels of the DMH. The DMH in the control brain is demarcated by dotted lines. The inner dotted lines demarcate the pars compacta. The outer and inner dotted lines in DMH-lesioned slices are replicated from those in control brain. Abbreviations: F, fornix; MMT, mammilothalamic tract. Scale bar: 1 mm.

were not significant (lesion size vs. locomotor anticipation on Day 7, $R = 0.679$, $P = 0.2418$; lesion size vs. locomotor anticipation on Day 14, $R = 0.079$, $P = 0.9108$; lesion size vs. preprandial temperature increase on Day 7, $R = -0.484$, $P = 0.1957$; lesion size vs. preprandial temperature increase on Day 14, $R = 0.108$, $P = 0.7905$).
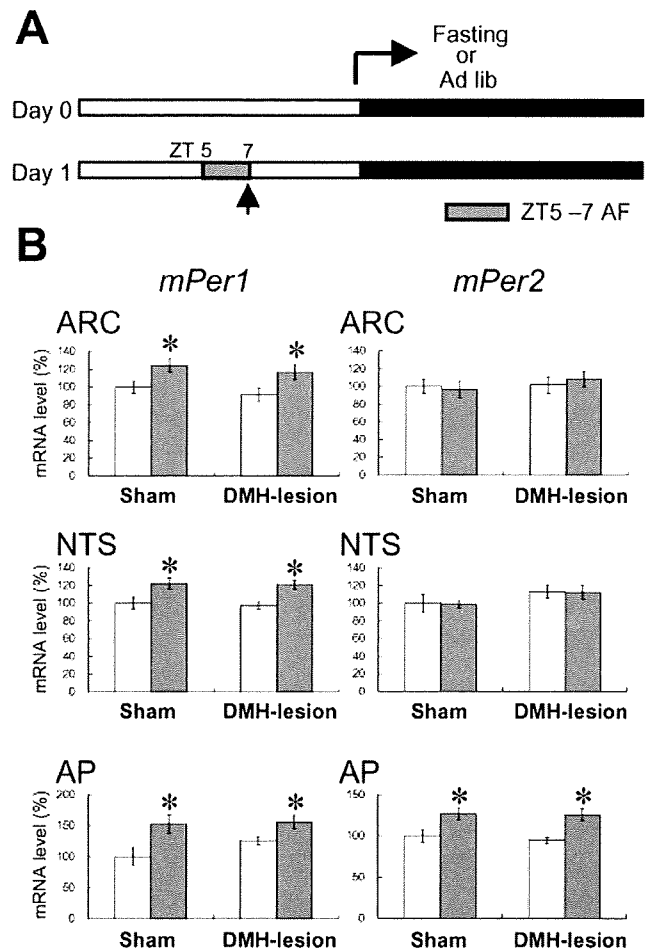
FIG. 6. Effects of DMH lesions on acute feeding-induced changes of *mPer1* and *mPer2* mRNA levels in the arcuate nucleus (ARC), nucleus of the solitary tract (NTS) and area postrema (AP). (A) Sampling schedules. Ten days after DMH lesion or sham operation, mice [gray column in (B)] were food-deprived overnight, refed from Zeitgeber time (ZT)5 to ZT7, and then decapitated. DMH and sham lesion mice fed *ad libitum* [open column in (B)] were decapitated at ZT7. (B) *mPer1* and *mPer2* mRNA levels in the ARC, NTS and AP. The values for *ad libitum* fed sham lesion mice were set to 100%. $*P < 0.05$ vs. *ad libitum* mice (Tukey–Kramer's test). Each group is made up of five–seven animals.

Discussion

The DMH has been proposed as the site of food-entrainable oscillators necessary and sufficient for the generation of food-anticipatory behavioral and temperature rhythms in rats. This proposal is based on findings that feeding schedules reset daily rhythms of clock gene expression in the mouse DMH (Mieda *et al.*, 2006), that partial DMH lesions attenuate or eliminate food-anticipatory rhythms in rats (Gooley *et al.*, 2006) and that virally mediated restoration of *BMAL1* expression only in the DMH is sufficient to rescue food-anticipatory rhythms in *BMAL1−/−* mice (Fuller *et al.*, 2008). However, the report of food-entrained clock gene rhythms in the DMH of mice had (until our study) not yet been confirmed, while attempts to confirm a critical role for the DMH or *BMAL1* in food-anticipatory rhythms in rats have so far produced no supportive evidence from four independent laboratories (Landry *et al.*, 2006, 2007; Mistlberger *et al.*, 2008; Storch & Weitz 2009; Pendergast *et al.*, 2009). The results of the present study also do not support a necessary role for the DMH. The results do confirm that
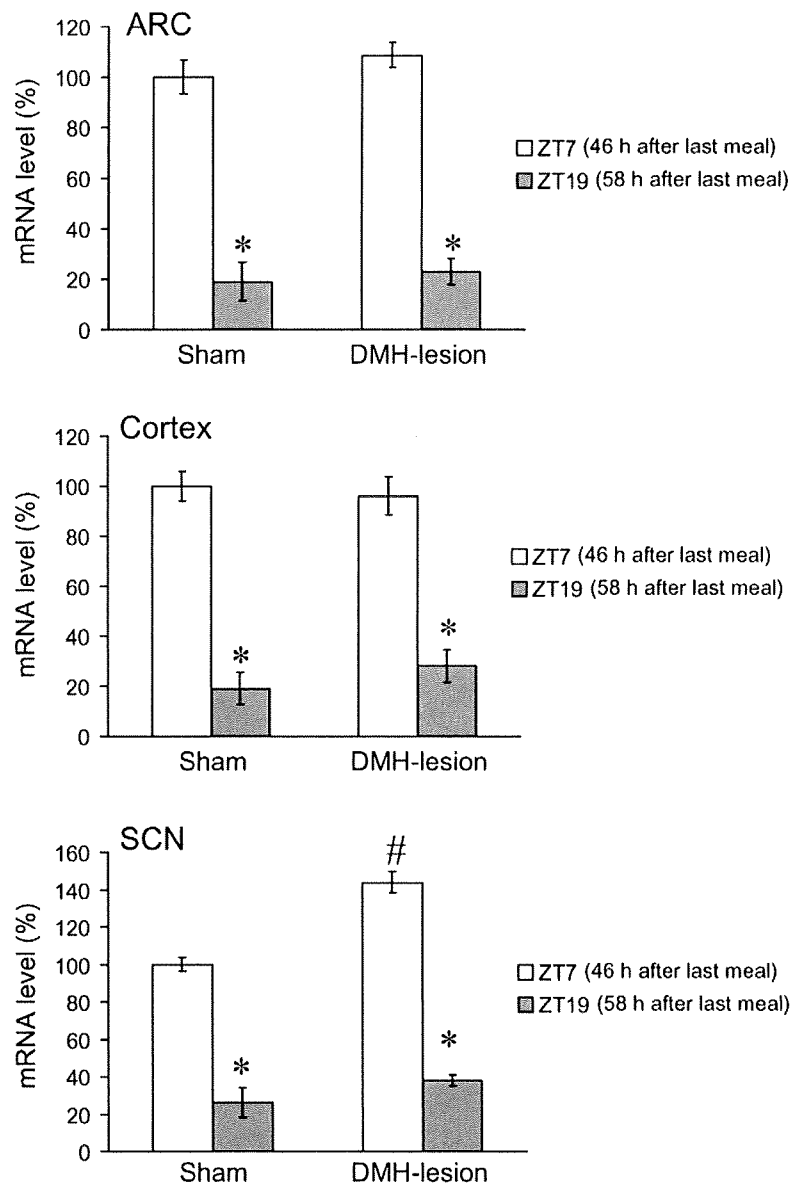
FIG. 7. Effects of DMH lesion on the daily expression of *mPer2* mRNA levels in the arcuate nucleus (ARC), cortex and suprachiasmatic nucleus (SCN) of mice on a daily restricted feeding schedule. After overnight fasting, sham-operated and DMH-lesioned mice received food from Zeitgeber time (ZT)5 to ZT9 for a total of 12 days (Day 1–Day 6 and Day 8–Day 13), and were withdrawn food on Days 7, 14 and 15. They were killed at ZT7 or ZT15 on Day 15. The values for control sham-operated mice at ZT7 are set to 100%. Each group is made up of three animals. *$P < 0.05$ vs. ZT7 (Student's t-test). #$P < 0.05$ vs. sham group (Student's t-test).

clock gene expression in the DMH exhibits a daily rhythm in mice maintained on restricted daytime feeding schedules. However, while the rhythm is particularly prominent in the DMH, it is not unique to this structure, and clock gene rhythms in other areas were not affected by DMH ablation. Moreover, although mice with total or near total DMH lesions were less active and tended to be less nocturnal during *ad libitum* food access, these mice showed essentially normal food-anticipatory rhythms of locomotor activity and core body temperature during restricted feeding. Notably, food-anticipatory rhythms persisted during meal omission days in both LD and DD. The results of this study therefore provide no evidence that putative circadian oscillators in the DMH play a role as a pacemaker driving food-entrainable rhythms of behavior, physiology or gene expression elsewhere in the brain.

The significance of daily rhythms of clock gene expression in the DMH remains to be clarified. The DMH may play a role as driving oscillator for other food-entrainable rhythms, such as autonomic or endocrine (e.g. corticosterone) activity. These will need to be assessed in future studies. Rhythms of DMH mPER2-immunoreactivity have been observed in rats anticipating a single midday feeding, but not in rats anticipating a palatable snack, although both feeding schedules were associated with food-anticipatory *cFos* expression in the DMH (Verwey *et al.*, 2007). Those results indicate that DMH neural activity correlates with food-anticipatory activity, but that DMH clock gene oscillations are reset only by caloric restriction. A prediction from these observations is that if DMH output drives any food-entrainable rhythms, these are most likely to be rhythms of neural or endocrine processes involved in metabolic adjustments to reduced caloric intake.
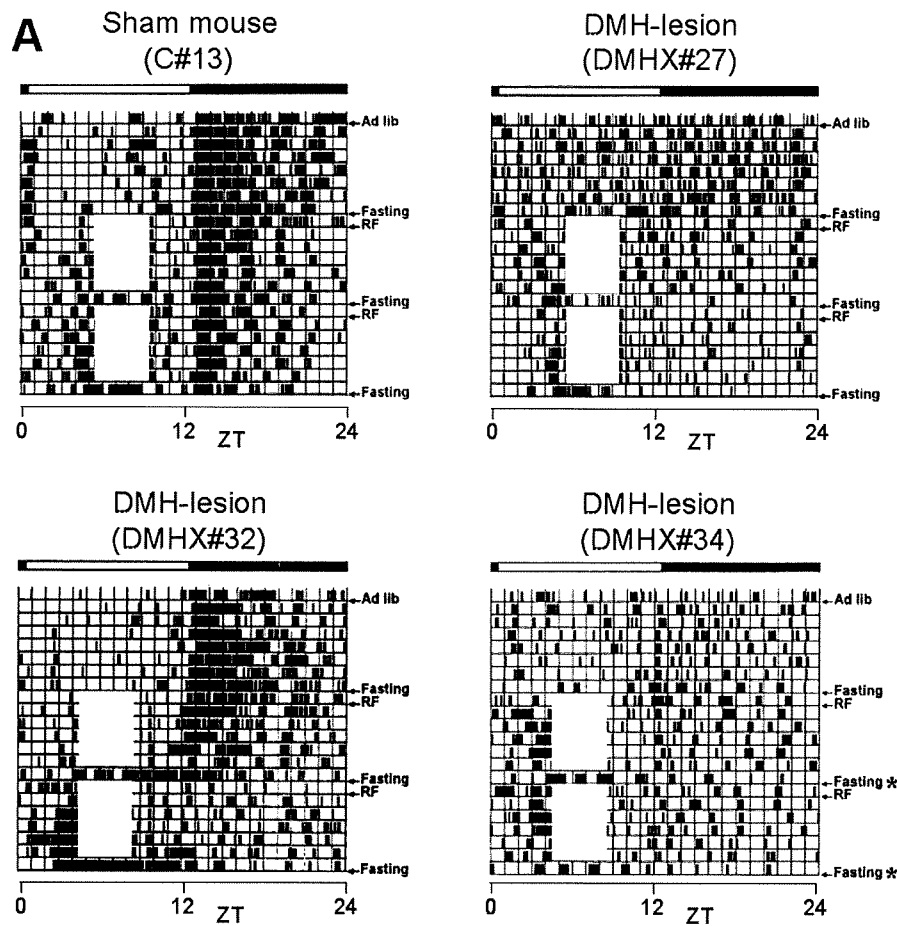
FIG. 8. Effects of dorsomedial hypothalamic nucleus (DMH) lesions on food anticipatory activity under light–dark (LD) and constant darkness (DD) conditions. (A) Representative single-plotted actograms of sham-operated control (C#13) and DMH-lesioned mice (DMHX#27, #32, #34). Mice of C#13, DMHX#27 and #32 were maintained in LD throughout the experiment, and DMHX#34 was maintained in LD during *ad libitum* and daily restricted feeding, and in DD during the meal omission days (7 and 14) as shown by asterisks. Each line represents 24 h, plotted in 6-min time bins from left to right. Dark vertical bars indicate time bins with activity counts. The plotting threshold was set to 1 count per 6-min time bins. Horizontal open and closed bars indicate the light and dark periods, respectively. Daily mealtime (ZT5–ZT9) during restricted feeding (RF) is indicated by the opaque boxes. (B) Group average waveforms of locomotor activity in sham-operated (open circles, *n* = 6) and DMH-lesioned mice (closed circles, *n* = 6) fed *ad libitum* (*Ad-lib*), on Day 2 (second day after RF start), Day 6 (sixth day after RF starts), Day 7 (food-withdrawal day), Day 13 (13th day after RF starts) and Day 14 (food-withdrawal day). Upper open and closed bars in each graph indicate the light and dark periods, respectively. Feeding times on Day 2, Day 6 and Day 13 are shown by horizontal gray bars. The hatched bars in the graphs for meal omission days (7 and 14) indicate the previous feeding time. Activity counts are expressed as % of the daily totals [(activity count per hour/total activity count for 24 h) × 100]. (C) Group average waveforms of locomotor activity in sham-operated (open circles, *n* = 5) and DMH-lesioned mice (closed circles, *n* = 5) with intraperitoneal temperature loggers. Mice in these groups were maintained in LD during *ad libitum* and daily restricted feeding, and in DD during the meal omission days (7 and 14).

Another possibility is that DMH oscillators do participate in driving food-anticipatory behavioral and temperature rhythms, but redundantly as part of a broader system of food-entrainable oscillators, distributed within the hypothalamus and elsewhere. Consistent with other reports, we observed significant food-evoked and food-entrained clock gene expression in several other areas, including the hypothalamic ARC. *In vitro*, the ARC from *per:luc* transgenic rats exhibits circadian rhythms of bioluminescence driven by the *Per2* gene promoter (Guilding *et al.*, 2008). These rhythms persisted for at least 2 days, and were more robust than rhythms detected in the DMH and PVN in the same hypothalamic slices. This has been taken to suggest a hierarchy of food-entrainable oscillators in the mediobasal hypothalamus (Guilding & Piggins, 2007). Although lesions of the ARC (Mistlberger & Antle, 1999), PVN (Mistlberger & Rusak, 1988) and DMH (Landry *et al.*, 2006, 2007) alone do not eliminate food-anticipatory activity rhythms, a lesion test of a combined role for these areas has not been done.

In the present study, we observed feeding-elicited transient induction of *mPer1* and/or *mPer2* gene expression not only in the DMH, but also in the NTS and the AP as reported previously (Mieda *et al.*, 2006). At present, we do not know the physiological significance of the transient *Per* induction in the DMH by feeding. Given that *Per1* and *Per2* are also rapidly induced in the SCN after a light pulse (Shigeyoshi *et al.*, 1997; Moriya *et al.*, 2000), and in cultured cells treated with various reagents capable of driving the circadian expression rhythms of clock-related genes (Balsalobre *et al.*, 1998), stimulation of *Per* genes (particularly *Per2*; Feillet *et al.*, 2006) may be critical for inducing or resetting food-entrainable oscillations in the brain.

To evaluate the role of the DMH in food-evoked and food-entrained rhythms in the present study, a large number of mice received DMH lesions. Only mice sustaining lesions > 80% were included in subsequent analyses. This screening criterion was based partly on Gooley *et al.*'s (2006) criterion for classifying DMH lesions as
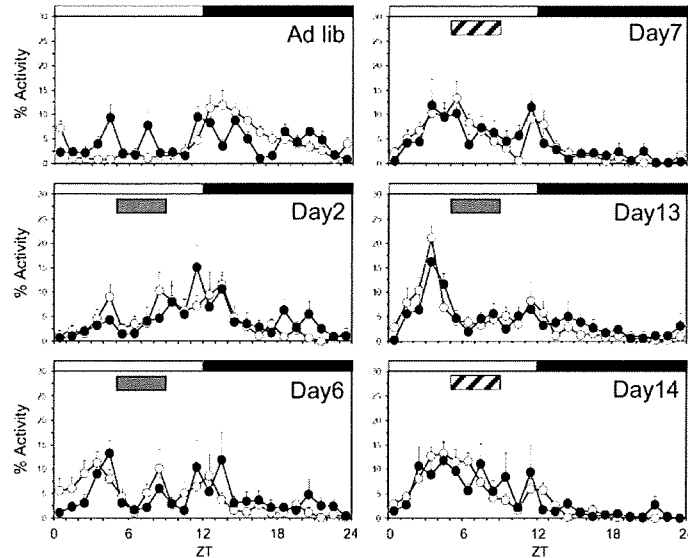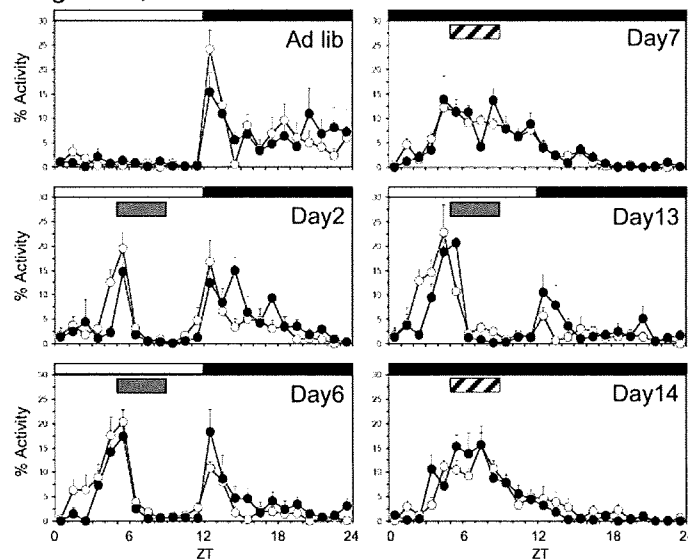
B Restricted feeding in LD, meal omission tests in LD

**C** Restricted feeding in LD, meal omission tests in DD

FIG. 8. (Continued)

complete, and partly on the evidence that the pars compacta, particularly caudally and medially, is the site of all or most clock gene expression in the DMH of mice and rats during food restriction (present study; Mieda *et al.*, 2006; Verwey *et al.*, 2007). By virtue of its size and location within the DMH, the pars compacta was bilaterally destroyed by DMH lesions estimated to be 80% or more complete. Gooley *et al.* (2006) reported in rats a linear correlation between the amount of DMH tissue damaged and the amplitude of food-anticipatory rhythms. If this is true in mice, then a group of mice with > 80% DMH ablation, and no remaining pars compacta, should exhibit both weaker and more variable anticipation by comparison with intact mice. However, we observed no such differences between groups of sham and DMH-lesion mice. Total daily activity levels were significantly reduced in DMH-lesion mice, but when activity data were normalized for differences in mean levels, sham and DMH-lesion groups showed virtually identical food-anticipatory rhythms, and

every DMH-lesion mouse exhibited food-anticipatory activity. Consequently, the lack of effect of DMH lesions on food-anticipatory rhythms cannot be attributed to the inclusion of mice with small portions of DMH spared.

In the SCN, the site of the master light-entrainable circadian clock, light-induced *Per1* and *Per2* expression can be blocked by NMDA antagonists (Shigeyoshi *et al.*, 1997; Moriya *et al.*, 2000; Asai *et al.*, 2001). In the present study, *mPer1* and *mPer2* expression in several brain regions were rapidly induced by midday feeding after an overnight fast, and in the DMH this was blocked by the NMDA antagonist +MK801 (other areas were not examined). This suggests similar mechanisms underlying induction of *mPer* genes in the SCN and DMH by photic and non-photic stimuli, respectively. By contrast, +MK801 did not affect *mPer1* and *mPer2* gene expression in the DMH after 6 days of restricted feeding. In contrast with the administration-sampling interval of 2.5 h in the acute experiment, we adopted the

A   Body temperature
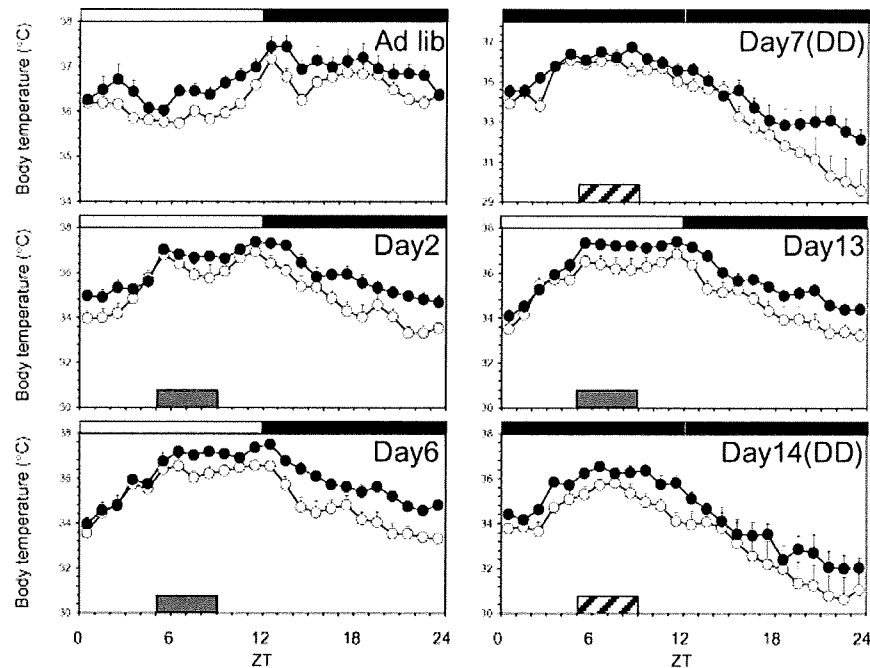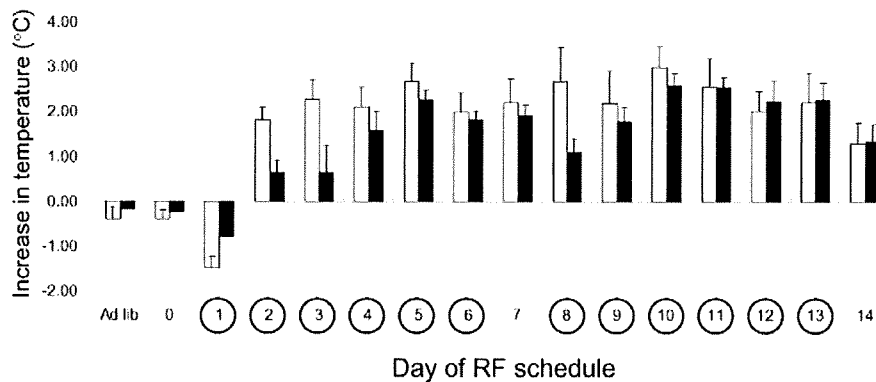

B   Preprandial increase in body temperature

Fig. 9. (A) Group average profiles of core body temperature in sham-operated (open circles, $n = 9$) and DMH-lesioned mice (closed circles, $n = 9$) during *ad libitum* (*Ad-lib*) food access, during restricted daytime (ZT5–ZT9) feeding (Days 2, 6, 13) in LD, and during meal omission days (Days 7, 14) in constant darkness (DD). Feeding times on Days 2, 6 and 13 are shown by horizontal gray bars. Previous feeding time on Days 7 and 14 (meal omission days) are indicated by the horizontal hatched bars. (B) Preprandial increase in body temperature in sham (open columns, $n = 9$) and DMH-lesioned mice (closed columns, $n = 9$). The increase in temperature was calculated by subtracting the averaged temperature during ZT0–ZT1 from those during ZT4–ZT5. The numbers in the circle indicate the day of restricted feeding.

procedure of the longer interval (7-h length, from drug injection at ZT0 and brain sampling at ZT7), as the circadian rise either in *mPer1* or *mPer2* mRNA in the DMH of food-entrained rats was observed especially between ZT0 and ZT7 (Fig. 2D). Considering that the plasma half-life of systemically injected MK801 in rodents was approximately 1 h (Hucker *et al.*, 1983), we can not exclude the possibility that the difference in the administration-sampling intervals between feeding-induced and feeding-entrained expression experiment could explain the differential effects of +MK801. Therefore, although activation of NMDA receptors appears necessary for acute induction of *mPer* expression, the evidence against a role in the rhythmic expression of

DMH *Per* genes is less solid. Furthermore, as we administered ± MK801 systemically (intraperitoneally), we do not know whether ± MK801 exerts its effects via acting in the DMH or elsewhere in the brain and body. Further experiments using direct intracranial infusion into the DMH will be required to resolve this matter.

A novel observation in the present study was that the day/night difference in *mPer2* mRNA expression in the SCN was augmented in DMH-lesioned mice on restricted daytime-feeding schedules, due to enhanced expression at ZT7, when *mPer2* mRNA is normally rising but not yet at peak levels. The meaning of this is uncertain, but it could point to a role for the DMH in modulating SCN

pacemaker amplitude or output. The rodent SCN actively promotes sleep and inhibits arousal during the rest phase of the circadian cycle (Mistlberger, 2005). Food-entrainable circadian oscillators driving anticipatory activity during the day must overcome this influence. A structure like the DMH, which is clearly sensitive to feeding schedules and caloric deprivation, could promote daytime food-anticipatory activity and resetting of other oscillators by inhibiting SCN output (Buijs et al., 2006; Mistlberger, 2006; Escobar et al., 2007). To reconcile this idea with the repeated failure of radiofrequency/thermal DMH lesions to attenuate daytime food anticipation in rats and mice, it must be further hypothesized that sleep-promoting (or arousal-suppressing) outputs from the SCN pass through the medial hypothalamic area as fibers of passage that are destroyed by radiofrequency/thermal lesions but spared by cell-specific neurotoxins. According to this model, daytime food-anticipatory activity would be attenuated by ibotenic acid DMH lesions sparing fibers of passage (Gooley et al., 2006), but would be unaffected by radiofrequency/thermal DMH lesions (present study; Landry et al., 2006, 2007) or by combined DMH–SCN ablation (eliminating both DMH inhibition of SCN and SCN inhibition of daytime activity; Acosta-Galvan et al., 2008). A modulatory role for the DMH, if substantiated, could accommodate apparently incompatible results and provide a functional context for DMH rhythms. Further study using cell-specific DMH lesions in mice will be required to address this issue.

Supporting information

Additional supporting information may be found in the online version of this article:

Fig. S1. Autoradiograms demonstrating the effect of acute feeding on mPer1 and mPer2 mRNA expression.

Fig. S2. Autoradiograms demonstrating the effect of restricted feeding on mRNA levels of mPer1 mPer2 and mBMAL1.

Fig. S3. Expression rhythms of mPer1, mPer2 and mBMAL1 mRNAs in the arcuate nucleus.

Fig. S4. Expression rhythms of mPer1, mPer2 and mBMAL1 mRNAs in the parietal cortex.

Fig. S5. Expression rhythms of mPer1, mPer2 and mBMAL1 mRNAs in the suprachiasmatic nucleus.

Fig. S6. Expression rhythms of mPER2 protein in the DMH.

Fig. S7. Cresyl violet-stained brain sections from DMH-lesioned mice.

Please note: Wiley-Blackwell are not responsible for the content or functionality of any supporting materials supplied by the authors. Any queries (other than missing material) should be directed to the corresponding author for the article.

Acknowledgements

Abbreviations

AP, area postrema; ARC, arcuate nucleus; CP, caudate putamen; CTX, parietal cortex; DD, constant darkness; DMH, dorsomedial hypothalamic nucleus; LD, light–dark; NMDA, N-methyl-D-aspartate; NTS, nucleus of solitary tract; Per, Period; PVN, hypothalamic paraventricular nucleus; SCN, suprachiasmatic nucleus; VMH, ventromedial hypothalamic nucleus; ZT, Zeitgeber time.

References

Abe, M., Herzog, E.D., Yamazaki, S., Straume, M., Tei, H., Sakaki, Y., Menaker, M. & Block, G.D. (2002) Circadian rhythms in isolated brain regions. J. Neurosci., 22, 350–356.

Acosta-Galvan, G., Moro Chao, H., Escobar-Briones, C. & Buijs, R.M. (2008) Importance of the interaction between the dorsomedial hypothalamic nucleus and the suprachiasmatic nucleus for the expression of the food anticipatory activity. Proc. Soc. Res. Biol. Rhythms, 11, 199.

Angeles-Castellanos, M., Mendoza, J. & Escobar, C. (2007) Restricted feeding schedules phase shift daily rhythms of c-Fos and protein Per1 immunoreactivity in corticolimbic regions in rats. Neuroscience, 144, 344–355.

Angeles-Castellanos, M., Salgado-Delgado, R., Rodriguez, K., Buijs, R.M. & Escobar, C. (2008) Expectancy for food or expectancy for chocolate reveals timing systems for metabolism and reward. Neuroscience, 155, 297–307.

Asai, M., Yamaguchi, S., Isejima, H., Jonouchi, M., Moriya, T., Shibata, S., Kobayashi, M. & Okamura, H. (2001) Visualization of mPer1 transcription in vitro: NMDA induces a rapid phase shift of mPer1 gene in cultured SCN. Curr. Biol., 11, 1524–1527.

Balsalobre, A., Damiola, F. & Schibler, U. (1998) A serum shock induces circadian gene expression in mammalian tissue culture cells. Cell, 93, 929–937.

Bellinger, L.L. & Bernardis, L.L. (2002) The dorsomedial hypothalamic nucleus and its role in ingestive behavior and body weight regulation: lessons learned from lesioning studies. Physiol. Behav., 76, 431–442.

Boulos, Z. & Terman, M. (1980) Food availability and daily biological rhythms. Neurosci. Biobehav. Rev., 4, 119–131.

Buijs, R.M., Chunxia, Y., Challet, E. & Escobar, C. (2006) Pathways of metabolic non-photic input to the suprachiasmatic nucleus interfere with light input to the SCN. Soc. Res. Biol. Rhythms Abstr., 10, 43.

Damiola, F., Le Minh, N., Preitner, N., Kornmann, B., Fleury-Olela, F. & Schibler, U. (2000) Restricted feeding uncouples circadian oscillators in peripheral tissues from the central pacemaker in the suprachiasmatic nucleus. Genes Dev., 14, 2950–2961.

Davidson, A.J. (2006) Search for the feeding-entrainable circadian oscillator: a complex proposition. Am. J. Physiol. Regul. Integr. Comp. Physiol., 290, R1524–1526.

De Matteo, R., Head, G.A. & Mayorov, D.N. (2006) Angiotensin II in dorsomedial hypothalamus modulates cardiovascular arousal caused by stress but not feeding in rabbits. Am. J. Physiol. Regul. Integr. Comp. Physiol., 290, R257–264.

Diaz-Munoz, M., Vazquez-Martinez, O., Aguilar-Roblero, R. & Escobar, C. (2000) Anticipatory changes in liver metabolism and entrainment of insulin, glucagon, and corticosterone in food-restricted rats. Am. J. Physiol. Regul. Integr. Comp. Physiol., 279, R2048–2056.

Escobar, C., Diaz-Munoz, M., Encinas, F. & Aguilar-Roblero, R. (1998) Persistence of metabolic rhythmicity during fasting and its entrainment by restricted feeding schedules in rats. Am. J. Physiol., 274, R1309–1316.

Escobar, C., Martinez-Merlos, M.T., Angeles-Castellanos, M., del Carmen Miñana, M. & Buijs, R.M. (2007) Unpredictable feeding schedules unmask a system for daily resetting ofbehavioural and metabolic food entrainment. Eur. J. Neurosci., 26, 2804–2814.

Feillet, C.A., Mendoza, J., Albrecht, U., Pevet, P. & Challet, E. (2008) Forebrain oscillators ticking with different clock hands. Mol. Cell. Neurosci., 37, 209–221.

Feillet, C.A., Ripperger, J.A., Magnone, M.C., Dulloo, A., Albrecht, U. & Challet, E. (2006) Lack of food anticipation in Per2 mutant mice. Curr. Biol., 16, 2016–2022.

Fuller, P.M., Lu, J. & Saper, C.B. (2008) Differential rescue of light- and food-entrainable circadian rhythms. Science, 320, 1074–1077.

Gooley, J.J. & Saper, C.B. (2007) Is food-directed behavior an appropriate measure of circadian entrainment to restricted daytime feeding? J. Biol. Rhythms, 22, 479–483.

Gooley, J.J., Schomer, A. & Saper, C.B. (2006) The dorsomedial hypothalamic nucleus is critical for the expression of food-entrainable circadian rhythms. Nat. Neurosci., 9, 398–407.

Grob, M., Trottier, J.F., Drolet, G. & Mouginot, D. (2003) Characterization of the neurochemical content of neuronal populations of the lamina terminalis activated by acute hydromineral challenge. Neuroscience, 122, 247–257.

Guilding, C. & Piggins, H.D. (2007) Challenging the omnipotence of the suprachiasmatic timekeeper: are circadian oscillators present throughout the mammalian brain? Eur. J. Neurosci., 25, 3195–3216.

Guilding, C., Hughes, A., Brown, T., Namvar, S. & Piggins, H. (2008) An ensemble of novel circadian oscillators in the mouse mediobasal hypothalamus. Comparative Biochemistry and Physiology Part A, 150, S149.

Hara, R., Wan, K., Wakamatsu, H., Aida, R., Moriya, T., Akiyama, M. & Shibata, S. (2001) Restricted feeding entrains liver clock without participation of the suprachiasmatic nucleus. *Genes Cells*, **6**, 269–278.

Hucker, H.B., Hutt, J.E., White, S.D., Arison, B.H. & Zacchei, A.G. (1983) Disposition and metabolism of (+)-5-methyl-10,11-dihydro-5H-dibenzo[a,d]cyclohepten-5,10-imine in rats, dogs, and monkeys. *Drug Metab. Dispos.*, **11**, 54–58.

Johnson, P.L. & Shekhar, A. (2006) Panic-prone state induced in rats with GABA dysfunction in the dorsomedial hypothalamus is mediated by NMDA receptors. *J. Neurosci.*, **26**, 7093–7104.

Landry, G.J. & Mistlberger, R.E. (2007) Food entrainment: methodological issues. *J. Biol. Rhythms*, **22**, 484–487.

Landry, G.J., Simon, M.M., Webb, I.C. & Mistlberger, R.E. (2006) Persistence of a behavioral food-anticipatory circadian rhythm following dorsomedial hypothalamic ablation in rats. *Am. J. Physiol. Regul. Integr. Comp. Physiol.*, **290**, R1527–1534.

Landry, G.J., Yamakawa, G.R., Webb, I.C., Mear, R.J. & Mistlberger, R.E. (2007) The dorsomedial hypothalamic nucleus is not necessary for the expression of circadian food-anticipatory activity in rats. *J. Biol. Rhythms*, **22**, 467–478.

Matsuo, T., Yamaguchi, S., Mitsui, S., Emi, A., Shimoda, F. & Okamura, H. (2003) Control mechanism of the circadian clock for timing of cell division in vivo. *Science*, **302**, 255–259.

Mieda, M., Williams, S.C., Richardson, J.A., Tanaka, K. & Yanagisawa, M. (2006) The dorsomedial hypothalamic nucleus as a putative food-entrainable circadian pacemaker. *Proc. Natl. Acad. Sci. U.S.A.*, **103**, 12150–12155.

Mistlberger, R.E. (1994) Circadian food-anticipatory activity: formal models and physiological mechanisms. *Neurosci. Biobehav. Rev.*, **18**, 171–195.

Mistlberger, R.E. (2005) Circadian regulation of sleep in mammals: role of the suprachiasmatic nucleus. *Brain Res. Brain Res. Rev.*, **49**, 429–454.

Mistlberger, R.E. (2006) Circadian rhythms: perturbing a food-entrained clock. *Curr. Biol.*, **16**, R968–969.

Mistlberger, R.E. & Antle, M.C. (1999) Neonatal monosodium glutamate alters circadian organization of feeding, food anticipatory activity and photic masking in the rat. *Brain Res.*, **842**, 73–83.

Mistlberger, R.E., Buijs, R.M., Challet, E., Escobar, C., Landry, G.J., Kalsbeek, A., Pevet, P. & Shibata, S. (2009b) Standards of evidence in chronobiology: Critical review of a report that restoration of Bmal1 expression in the dorsomedial hypothalamus is sufficient to restore circadian food anticipatory rhythms in Bmal1-/- mice. *J. Circadian Rhythms*, in press.

Mistlberger, R.E. & Rusak, B. (1988) Food anticipatory circadian rhythms in paraventricular and lateral hypothalamic lesioned rats. *J. Biol. Rhythms*, **3**, 277–292.

Mistlberger, R.E., Yamazaki, S., Pendergast, J.S., Landry, G.J., Takumi, T. & Nakamura, W. (2008) Comment on "Differential rescue of light- and food-entrainable circadian rhythms". *Science*, **322**, 675.

Mistlberger, R.E., Kent, B.A. & Landry, G.J. (2009a) Phenotyping food-entrainment: motion sensors and telemetry are equivalent. *J. Biol. Rhythms*, **24**, 95–98.

Pendergast, J.S., Nakamura, W., Friday, R.C., Hatanaka, F., Takumi, T., & Yamazaki, S. (2009) Robust food anticipatory activity in BMAL1-deficient mice. *PLoS One*, in press.

Morgado, E., Gordon, M.K., del Carmen Minana-Solis, M., Meza, E., Levine, S., Escobar, C. & Caba, M. (2008) Hormonal and metabolic rhythms associated with the daily scheduled nursing in rabbit pups. *Am. J. Physiol. Regul. Integr. Comp. Physiol.*, **295**, R690–695.

Moriya, T., Horikawa, K., Akiyama, M. & Shibata, S. (2000) Correlative association between N-methyl-D-aspartate receptor-mediated expression of period genes in the suprachiasmatic nucleus and phase shifts in behavior with photic entrainment of clock in hamsters. *Mol. Pharmacol.*, **58**, 1554–1562.

Ono, M., Shibata, S., Minamoto, Y. & Watanabe, S. (1996) Effect of the noncompetitive N-methyl-D-aspartate (NMDA) receptor antagonist MK-801 on food-anticipatory activity rhythm in the rat. *Physiol. Behav.*, **59**, 585–589.

Richard, D. & Bourque, C.W. (1992) Synaptic activation of rat supraoptic neurons by osmotic stimulation of the organum vasculosum lamina terminalis. *Neuroendocrinology*, **55**, 609–611.

Shigeyoshi, Y., Taguchi, K., Yamamoto, S., Takekida, S., Yan, L., Tei, H., Moriya, T., Shibata, S., Loros, J.J., Dunlap, J.C. & Okamura, H. (1997) Light-induced resetting of a mammalian circadian clock is associated with rapid induction of the mPer1 transcript. *Cell*, **91**, 1043–1053.

Stephan, F.K. (2002) The "other" circadian system: food as a Zeitgeber. *J. Biol. Rhythms*, **17**, 284–292.

Stephan, F.K., Swann, J.M. & Sisk, C.L. (1979) Entrainment of circadian rhythms by feeding schedules in rats with suprachiasmatic lesions. *Behav. Neural. Biol.*, **25**, 545–554.

Stokkan, K.A., Yamazaki, S., Tei, H., Sakaki, Y. & Menaker, M. (2001) Entrainment of the circadian clock in the liver by feeding. *Science*, **291**, 490–493.

Storch, K.F. & Weitz, C.J. (2009) Daily rhythms of food anticipatory activity do not require the known circadian clock. *Proc. Natl. Acad. Sci. USA.*, in press.

Thompson, R.H. & Swanson, L.W. (1998) Organization of inputs to the dorsomedial nucleus of the hypothalamus: a reexamination with Fluorogold and PHAL in the rat. *Brain Res. Brain Res. Rev.*, **27**, 89–118.

Thompson, R.H., Canteras, N.S. & Swanson, L.W. (1996) Organization of projections from the dorsomedial nucleus of the hypothalamus: a PHA-L study in the rat. *J. Comp. Neurol.*, **376**, 143–173.

Verwey, M., Khoja, Z., Stewart, J. & Amir, S. (2007) Differential regulation of the expression of Period2 protein in the limbic forebrain and dorsomedial hypothalamus by daily limited access to highly palatable food in food-deprived and free-fed rats. *Neuroscience*, **147**, 277–285.

Waddington Lamont, E., Harbour, V.L., Barry-Shaw, J., Renteria Diaz, L., Robinson, B., Stewart, J. & Amir, S. (2007) Restricted access to food, but not sucrose, saccharine, or salt, synchronizes the expression of Period2 protein in the limbic forebrain. *Neuroscience*, **144**, 402–411.

Wakamatsu, H., Yoshinobu, Y., Aida, R., Moriya, T., Akiyama, M. & Shibata, S. (2001) Restricted-feeding-induced anticipatory activity rhythm is associated with a phase-shift of the expression of mPer1 and mPer2 mRNA in the cerebral cortex and hippocampus but not in the suprachiasmatic nucleus of mice. *Eur. J. Neurosci.*, **13**, 1190–1196.

Weaver, D.R. (1998) The suprachiasmatic nucleus: a 25-year retrospective. *J. Biol. Rhythms*, **13**, 100–112.

Phospholipase C-β4 Is Essential for the Progression of the Normal Sleep Sequence and Ultradian Body Temperature Rhythms in Mice

Masayuki Ikeda[1,2,3]*, Moritoshi Hirono[2,4], Takashi Sugiyama[2¤], Takahiro Moriya[2,5], Masami Ikeda-Sagara[1], Naomi Eguchi[3], Yoshihiro Urade[3], Tohru Yoshioka[2,6]

1 Department of Chronobiology, Graduate School of Innovative Life Science, University of Toyama, Toyama, Japan, 2 Department of Molecular Neurobiology, Advanced Institute for Biological Science, Waseda University, Tokyo, Japan, 3 Department of Molecular Behavioral Biology, Osaka Bioscience Institute, Osaka, Japan, 4 Yamada Research Unit, RIKEN Brain Science Institute, Saitama, Japan, 5 Department of Cellular Signaling, Graduate School of Pharmaceutical Sciences, Tohoku University, Sendai, Japan, 6 Center of Excellent for Environmental Medicine, Graduate Institute of Medical Sciences, Kaohsiung Medical University, Kaohsiung, Taiwan

Abstract

Background: The sleep sequence: i) non-REM sleep, ii) REM sleep, and iii) wakefulness, is stable and widely preserved in mammals, but the underlying mechanisms are unknown. It has been shown that this sequence is disrupted by sudden REM sleep onset during active wakefulness (i.e., narcolepsy) in orexin-deficient mutant animals. Phospholipase C (PLC) mediates the signaling of numerous metabotropic receptors, including orexin receptors. Among the several PLC subtypes, the β4 subtype is uniquely localized in the geniculate nucleus of thalamus which is hypothesized to have a critical role in the transition and maintenance of sleep stages. In fact, we have reported irregular theta wave frequency during REM sleep in PLC-β4-deficient mutant (PLC-β4−/−) mice. Daily behavioral phenotypes and metabotropic receptors involved have not been analyzed in detail in PLC-β4−/− mice, however.

Methodology/Principal Findings: Therefore, we analyzed 24-h sleep electroencephalogram in PLC-β4−/− mice. PLC-β4−/− mice exhibited normal non-REM sleep both during the day and nighttime. PLC-β4−/− mice, however, exhibited increased REM sleep during the night, their active period. Also, their sleep was fragmented with unusual wake-to-REM sleep transitions, both during the day and nighttime. In addition, PLC-β4−/− mice reduced ultradian body temperature rhythms and elevated body temperatures during the daytime, but had normal homeothermal response to acute shifts in ambient temperatures (22°C–4°C). Within the most likely brain areas to produce these behavioral phenotypes, we found that, not orexin, but group-1 metabotropic glutamate receptor (mGluR)-mediated Ca^{2+} mobilization was significantly reduced in the dorsal lateral geniculate nucleus (LGNd) of PLC-β4−/− mice. Voltage clamp recordings revealed that group-1 mGluR-mediated currents in LGNd relay neurons (inward in wild-type mice) were outward in PLC-β4−/− mice.

Conclusions/Significance: These lines of evidence indicate that impaired LGNd relay, possibly mediated via group-1 mGluR, may underlie irregular sleep sequences and ultradian body temperature rhythms in PLC-β4−/− mice.

Introduction

The behavioral state of sleep consists of two basic stages: (1) rapid-eye-movement (REM) sleep with typical theta electroencephalogram (EEG) waves and (2) restful non-REM sleep, with slow EEG waves. The sleep sequence: i) non-REM sleep, ii) REM sleep, and iii) wakefulness, is stable and widely preserved in mammals, with REM sleep consistently following non-REM sleep. While understanding of the REM-regulating network remains incomplete, it is known that in general, the occurrence of REM sleep follows the generation of ponto-geniculo-occipital waves that arise in the pons

and are transmitted to the thalamic lateral geniculate nucleus (LGN) and visual occipital cortex. The REM-On neurons in the laterodorsal and pedunculopontine tegmental nuclei under the regulation of serotonergic dorsal raphe neurons and noradrenergic locus coeruleus neurons may be critical for the activation of the pontine reticular formation (PRF) and ultimately contribute to the shift to REM sleep [1,2]. However, understanding of the REM-regulating network is incomplete due to the large network size.

Narcolepsy is characterized by sudden REM sleep attacks during active wakefulness, and thus represents a rare condition in which the preserved sleep sequence is disrupted. Orexin receptor

mutations are the cause of canine narcolepsy [3], and orexin knockout mice displayed behaviors resembling aspects of narcolepsy [4–6], suggesting that orexinergic neuronal transmission is an essential component of the preserved sleep sequence. Orexin may regulate REM sleep within the PRF since perfusion of antisense oligonucleotides for the orexin-2 receptor into the PRF produces irregular REM sleep similar to that of orexin knockout mice [7]. On the other hand, orexin receptive neurons are densely distributed in the locus coeruleus [8] and thalamic rhomboid and centromedial nuclei [9,10], where they may receive projections from the PRF. There are multiple and diverse orexinergic projections in the brain [11], and the specific orexin projection responsible for the disruption of the sleep sequence in orexin-deficient mutant animals has not been elucidated.

Phospholipase C (PLC) is an enzyme that mediates cellular signaling via various metabotropic receptors. Orexin-1 and -2 receptors are metabotropic receptors, presumably linked to PLC [12]. To date, several PLC subtypes have been cloned and the β4 subtype is located in the cerebellum [13,14] and visual input pathways such as retina [15], superior colliculus, and thalamic geniculate nucleus [16]. The thalamic geniculate nucleus is also part of the sleep-regulating system, and exhibits robust expression of PLC-β4, especially in the dorsal LGN (LGNd)[16], where pontomedullary sleep-regulating neurons terminate. LGNd relay neurons are also part of a corticothalamic feedback loop, which is hypothesized to have a critical role in the transition of sleep stages [17–19]. We have reported irregular EEG power spectrum during REM sleep in PLC-β4-deficient mutant (PLC-β4−/−) mice when it was analyzed randomly from their sleep EEG [16]. Here, we further investigate possible roles of PLC-β4 in daily sleep-wake and body temperature rhythms.

Materials and Methods

Sleep Recording

Methods for the creation of PLC-β4−/− mice were described previously [13]. Also, sleep-wake stages of mice were analyzed based on EEG and electromyogram (EMG) as described previously [20]. Briefly, 12–15 weeks old male wild-type C57BL6J mice ($n = 6$) and PLC-β4−/− mice ($n = 6$) were used in the experiments. The PLC-β4−/− mice were littermates intercrossed between male and female heterozygotes that were backcrossed to C57BL6J mice for at least seven generations. The animals were maintained under a 12-hour light/dark cycle in sound-attenuated temperature-controlled ($22.0 \pm 1.0°C$) chambers. Mice were deeply anesthetized with pentobarbital (50 mg/kg, i.p.) and implanted with two EEG electrodes over the parietal cortex and the cerebellum. Two EMG electrodes were inserted in the muscle of the dorsal neck. Animals were allowed at least 10 days of recovery from surgery, and after habituation to experimental conditions, three consecutive 24-hour recordings.

The vigilance states were automatically classified off-line by 4-second epochs into three stages of wake, non-REM, and REM sleep by SLEEPSIGN (Kissei COMTEC, Matsumoto, Japan), according to the standard criteria [20,21]. As a final step, defined sleep–wake stages were examined visually, and corrected, if necessary. The sleep scoring data on the second day were used for further statistical comparisons.

Measurement of Body Temperature Rhythms

Animals were anesthetized by an intraperitoneal injection of pentobarbital (50 mg/kg, i.p.) for abdominal surgery. A telemetry probe was implanted intraperitoneally in wild type mice (n = 5) and PLC-β4−/− mice (n = 5). After 10 days recovery, the body

temperature was continuously monitored at 5 minute intervals for 3 weeks using a telemetry system (Dataquest LabPRO ver. 3.10, Data Sciences International, St. Paul, MN). Daily variations in body temperature levels were averaged from data recorded for three consecutive days on the second week of monitoring. During the recording period, food and water were given *ad libitum* and mice were kept under a 12-h light/dark cycle at $22.0 \pm 1.0°C$. To analyze homeostatic thermal regulation, wild-type (n = 4) and PLC-β4−/− mice (n = 4) were transferred for 2 hours to a cage with a reduced temperature ($4.0 \pm 1.0°C$) during the light period. The above *in vivo* recording experiments were designed to minimize the number of animals used and their suffering based on international guidelines and were approved by the appropriate animal care and use committees at Osaka Bioscience Institute and Waseda University.

Immunocytochemistry

Affinity-purified rabbit polyclonal antibodies for PLC-β1, -β2, -β3 and -β4 (Santa Cruz Biotechnology, Santa Cruz, CA) were used. One month old mice were anesthetized with pentobarbital and transcardially perfused with 4% phosphate-buffered paraformaldehyde (4°C; pH 7.4). The brains were immersed overnight in the fixative and embedded in paraffin and sectioned at 4 μm thick. As a blocking step, the sections were incubated with 3% H_2O_2 distilled water for 10 minutes, and 10% normal goat serum for 1 hour. The antibodies against PLC-β1 (1/500), PLC-β2 (1/500), PLC-β3 (1/100) or PLC-β4 (1/50) were applied to sections overnight at 4°C. Subsequently, sections were incubated with biotin-conjugated goat anti-rabbit IgG (Vector Laboratories, Burlingame, CA) for 1 hour at room temperature. Sections were then incubated with peroxidase-conjugated streptoavidin (Nichirei, Tokyo, Japan) for 1 hour at room temperature. Between each incubation step the sections were rinsed twice in 0.01 M phosphate-buffered saline (pH 7.4) for 5 minutes. The final peroxidase reaction was performed using 0.05% diaminobenzidine and 0.005% H_2O_2. The same sections were also stained with cresyl violet using conventional methods.

Ca^{2+} Imaging

Macroscopic Ca^{2+} imaging was performed as described previously [22]. Briefly, coronal slices (200 μm) containing the geniculate nuclei and hippocampus were prepared using a vibrating blade microtome in ice-cold high-Mg^{2+} (4 mM) and low-Ca^{2+} (0.5 mM) artificial cerebrospinal fluid (ACSF) bubbled with 95% O_2/5% CO_2. The slices were incubated for 3–5 hours in regular ACSF (2.5 mM CaCl$_2$ and 1 mM MgCl$_2$) bubbled with 95% O_2/5% CO_2. For Ca^{2+} imaging, the slices were immersed for 1 hour in regular ACSF containing 10 μM fura-2 AM (Molecular Probes, Eugene, OR) and 0.001% Cremophore El (Sigma). After washing out the fura-2 AM solution with ACSF, slices were placed in a glass-bottom chamber for optical measurements. Images were obtained at 10-second intervals using an upright microscope (Axioplan2; Carl Zeiss, Thornwood, NY). The intensity ratio in the region of interest was analyzed using a digital imaging system (Hamamatsu Photonics, Hamamatsu, Japan). (RS)-3,5-dihydroxy-phenylglycine (DHPG), 1S,3R-1-aminocyclopentane-1,3-dicarboxylic acid (1S, 3R-ACPD), orexin A, or orexin B (Sigma-RBI, St. Louis, MO) was applied for 1 minute by switching the perfusate (regular ACSF supplemented with 1 μM tetrodotoxin). The 50 mM K$^+$ ACSF was perfused for 45 seconds to estimate the maximal Ca^{2+} response.

Electrophysiology

Whole-cell voltage-clamp recordings were made from relay neurons (cell body diameter = 15–25 μm)[23] and interneurons

— 220 —

(≅ 10 μm)[24] in LGNd slices under Nomarski optics using a water-immersion objective (Achroplan 63×/0.90 w, Carl Zeiss). Patch pipettes (3–5 MΩ) were filled with intracellular solution containing 150 mM $CsCH_3SO_3$, 5 mM KCl, 0.1 mM K-EGTA, 5.0 mM Na-HEPES, 3.0 mM Mg-ATP, and 0.4 mM Na-GTP (pH 7.4). Membrane currents were recorded using an EPC-7 amplifier (List Electronic, Darmstadt, Germany) and pCLAMP software (Molecular Devices, Sunnyvale, CA), digitized, and stored on a diskette for later analysis. The series resistance compensation control of the amplifier was set at 50–70%. DHPG and α-amino-3-hydroxy-5-methyl-4-isoxazolepropionic acid (AMPA, Sigma-RBI) were applied in the vicinity of neurons via a Y-tube circulating regular ACSF supplemented with 1 μM tetrodotoxin. All experiments were performed at room temperature. Further details were described previously [13]. The above *in vitro* recording experiments were approved by the appropriate animal care and use committees at Waseda University and University of Toyama.

Statistical Analysis

All data are presented as means with standard errors. A two-tailed Student's *t*-test was used for the genotype-wise comparisons.

Results

Sleep Abnormality in PLC-β4−/− Mice

The length of non-REM sleep in PLC-β4−/− mice (352.9±14.9 minutes during the day and 207.7±29.9 minutes during the night, n = 6) was not significantly different from that in wild-type mice (365.4±19.0 minutes during the day and 187.5±15.7 minutes during the night, n = 6, n.s. by Student's *t*-test). Also, both genotypes exhibited similar delta (0.75–4.0 Hz) power density in the EEG spectrum during non-REM sleep (data not shown). PLC-β4−/− mice, however, exhibited arrhythmic REM sleep occurrences throughout their circadian cycle (Fig. 1A). Although the length of daytime REM sleep in PLC-β4−/− mice (51.1±4.7 minutes, n = 6) was not significantly different from that in wild-type mice (63.6±6.0 minutes, n = 6, n.s. by Student's *t*-test), the length of nighttime REM sleep in PLC-β4−/− mice (46.7±6.9 minutes, n = 6) was increased 80% over that in wild-type mice (25.3±3.2 minutes, n = 6, P<.01 by Student's *t*-test). Also, in PLC-β4−/− mice, episodes of REM sleep interrupted by wakefulness frequently were immediately followed by another REM episode, creating an unusual sleep sequence with REM-sleep/wakefulness repeats (Fig. 1B,C). Single short transitions from wakefulness to REM sleep were observed both in the wild type (2.7±0.4 times for 24 hours, n = 6) and PLC-β4−/− mice (3.5±0.5 times for 24 hours, n = 6, n.s. by Student's *t*-test). Sets of more than 3 REM sleep/wakefulness repeats (Fig. 1B), however, occurred only in PLC-β4−/− mice both during the day (6.0±0.6 sets, n = 6) and the night (6.5±1.5 sets, n = 6). These results clearly demonstrate that the mechanism underlying the progression of the proper sleep sequence is impaired in PLC-β4−/− mice.

Reduced Ultradian Body Temperature Rhythms in PLC-β4−/− Mice

Since the sleep-wake cycles generally couple to body temperature rhythms, we next analyzed abdominal temperature rhythms in PLC-β4−/− mice. Regardless of the genotypes, circadian rhythms in abdominal temperature levels were synchronized to light-dark cycles being high during the nighttime and low during the daytime (Fig. 2A–C). Although this circadian synchronization is intact in the PLC-β4−/− mice, daytime temperature levels were significantly higher in PLC-β4−/− mice (36.9±0.1°C, n = 5) than that in wild type mice (36.0±0.1°C, n = 5, P<.01 by

Student's t-test). The elevation in abdominal temperature levels depended on the circadian phase, since nighttime temperature levels were not different between PLC-β4−/− (37.3±0.1°C, n = 5) and wild type (37.4±0.1°C, n = 5). Coupling to the elevation of daytime temperature levels, ultradian (i.e., 2–3 hour periodic) temperature rhythms, which are observed frequently in the wild type mice, were significantly suppressed in PLC-β4−/− mice (Fig. 2A). To further analyze possible involvement of PLC-β4 in the thermoregulatory systems, mice were exposed to reduced (4°C) ambient temperature levels for 2 hours during the daytime. However, both genotypes displayed normal homeothermal response against shifts of ambient temperature (maximal temperature reduction = −1.5±0.8°C for PLC-β4−/− mice and −1.1±0.7°C for the wild type mice; n = 4 for both genotypes; n.s. by Student's *t*-test; Fig. 2D).

Localization of PLC-β4 in the Brain

The immunohistochemistry was used to analyze the expression of PLC-β4 in the mouse brain and confirmed successful gene knockout in the mice (Fig. 3A). While PLC-β1 and -β3 were expressed throughout the brain (Fig. 3B), PLC-β4 was predominately expressed in the cerebellum, thalamic geniculate nucleus, lateral posterior nucleus (LP), and superior colliculus (Sc) (Fig. 3A,B). Among these loci, the thalamic geniculate nucleus had one of the most robust expressions of PLC-β4, especially in the medial geniculate nucleus (MGN) and LGNd (Fig. 3B).

PLC-β4 Primarily Couples Group-1 mGluR in the LGNd

We first examined the effects of orexin-A (300 nM) and -B (300 nM). However, no intracellular Ca^{2+} was mobilized in response to activation of either orexin receptor type in any LGNd slice examined (number of slices = 12; Fig. 4A). Also, application of either the muscarinic acetylcholine receptor agonist, McNA343 (100 μM), or the H_1 histamine receptor agonist, HTMT (100 μM), failed to mobilize detectable intracellular Ca^{2+} in the LGNd (data not shown).

On the other hand, the group-1 mGluR agonist, DHPG (100 μM) significantly increased intracellular Ca^{2+} in all LGNd slices examined (number of slices = 6; Fig. 4B,C). DHPG produced significantly smaller Ca^{2+} increases (38.5% of the response in wild-type mice; P<.01 by Student's *t*-test) in the LGNd of PLC-β4−/− mice (Fig. 4B,C). DHPG also induced a slight decrease in Ca^{2+} after the increase in Ca^{2+} (Fig. 4B). The effects of the non-specific mGluR agonist, 1S,3R-ACPD (100 μM) were also examined to estimate the total mGluR response in the LGNd. In slices from wild-type mice, 1S,3R-ACPD produced a bi-phasic Ca^{2+} mobilization with a Ca^{2+} increase and subsequent Ca^{2+} decrease in the LGNd, whereas only the Ca^{2+} increase was observed in the dentate gyrus/CA3 region of the hippocampus (Fig. 4B,C). The Ca^{2+} increase in the LGNd was 39.9±3.8% smaller in amplitude than that in the dentate gyrus/CA3 region (number of slices = 6, P<.01 by Student's *t*-test). In slices from PLC-β4−/− mice, 1S,3R-ACPD produced only Ca^{2+} decreasing response in the LGNd, whereas the Ca^{2+} increasing response was intact in the dentate gyrus/CA3 region of the hippocampus (Fig. 4B,C).

PLC-β4 Couples Group-1 mGluR Signaling Primarily in Relay Neurons Not in Interneurons

To examine single-cellular group-1 mGluR responses in the LGNd, we recorded activity in the relay neurons and the interneurons separately using whole-cell patch clamp (Fig. 5). DHPG-induced inward currents in interneurons tended to be smaller in PLC-β4−/− mice (12.3±2.5 pA, n = 11) than those in wild-type
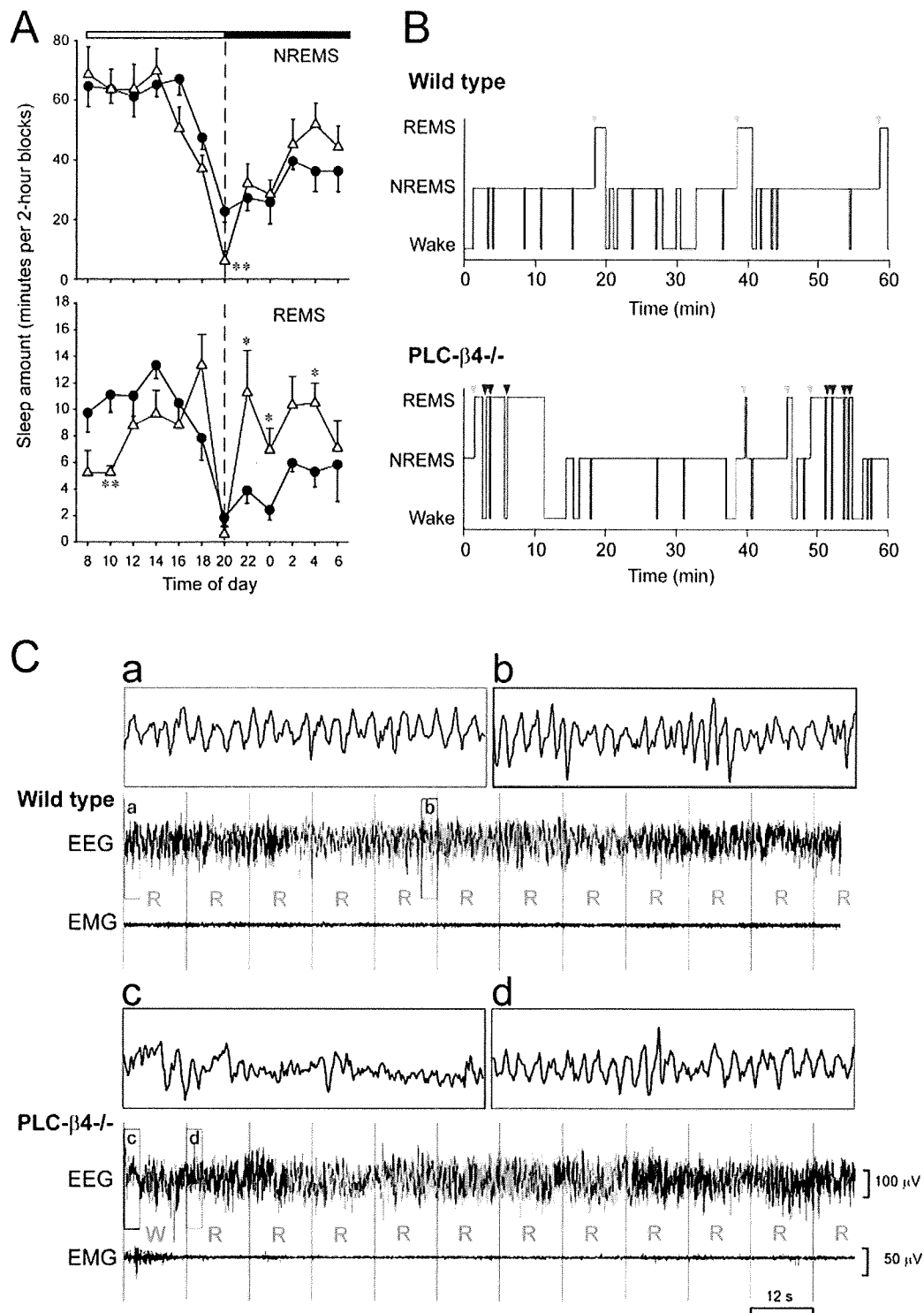
— 221 —

Figure 1. Sleep abnormality in PLC-β4−/− mice. A. The time courses of non-REM sleep (NREMS) and REM sleep (REMS) were plotted in 2 hour intervals for wild-type mice (n = 6, closed circles) and PLC-β4−/− mice (n = 6, open triangles). There was no difference in the time course of non-REM sleep except for a significant loss of sleep at the onset of darkness in PLC-β4−/− mice. The circadian time course of REM sleep was eliminated in PLC-β4−/− mice. *P<.05; **P<.01 compared with the corresponding wild-type group by Student's *t*-test. **B.** Hypnographic analysis also indicated abnormal REM sleep episodes in PLC-β4−/− mice. REM sleep regularly occurred after non-REM sleep in wild-type mice (the regular onset of REM sleep is marked by green arrows) whereas REM sleep episodes with frequent bouts of wakefulness were observed in PLC-β4−/− mice (REM sleep onset after wakefulness is marked by red arrows). **C.** *Upper.* An example sleep polygraph (combination of EEG and EMG) during regular REM sleep in a wild type mouse. *Lower.* An example sleep polygraph showing direct REM sleep transition from wakefulness in a PLC-β4−/− mouse. Squared 3-second EEG waves (**a-d**) were enlarged on the top. Typical theta waves were observed during both regular (**a,b**) and irregular (**d**) REM sleep. Estimated sleep stages are presented in 12-second bins. W: wakefulness, R: REM sleep.
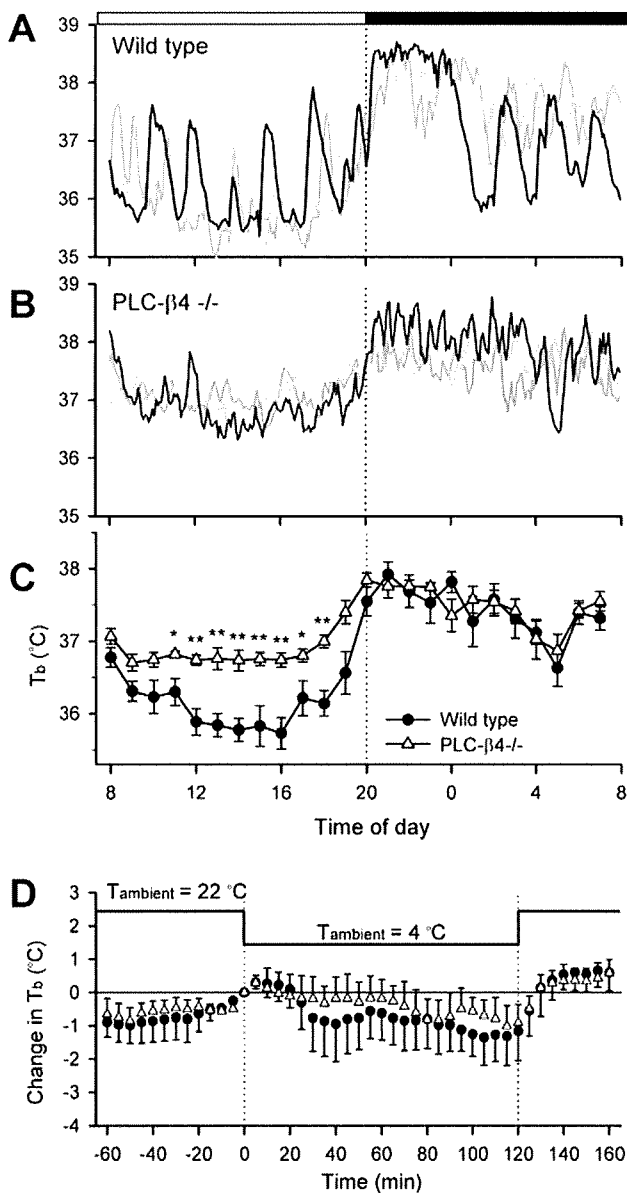doi:10.1371/journal.pone.0007737.g001

4

Figure 2. Reduced ultradian body temperature rhythms in PLC-β4−/− mice. Abdominal temperatures were measured in wild-type mice (A) and PLC-β4−/− mice (B) using a telemetry system. Representative abdominal temperature rhythms in 3 animals were plotted for each genotype. Although circadian rhythms of the temperature rhythm were manifest in both the wild-type and knockout mice, ultradian (i.e., 2–3 hour) oscillations were reduced in the knockout mice. White and black bars at the top denote light and dark periods. **C.** The temperature rhythm (±S.E.M.) was calculated for wild-type and PLC-β4−/− mice (n = 5 each). The daytime body temperature was significantly higher in the knockout mice than in the wild-type mice. *P<.05; **P<.01 compared with the corresponding wild-type group by Student's t-test. **D.** The ambient temperature was reduced from 22°C to 4°C for 2 hours to analyze the homeostatic thermal regulation in mice. No significant differences in the adaptive responses were found between the wild-type (n = 4, closed circle) and knockout (n = 4, open triangle) mice.
doi:10.1371/journal.pone.0007737.g002

mice (22.6±5.6 pA, n = 7), but the difference was not statistically significant (P = .07 by Student's t-test). On the other hand, DHPG induced outward currents in relay neurons in PLC-β4−/− mice, whereas AMPA induced inward currents similar in both genotypes.

Discussion

The results of the present study demonstrate that PLC-β4−/− mice exhibited increased REM sleep during the night and unusual wake-to-REM sleep transitions. Immunoreactivity to PLC-β4 was detected in the thalamus, superior colliculus, and cerebellum in mouse brain, with the highest expression levels in the thalamus observed in the LGNd and MGN (Fig. 3). To our knowledge, there is currently no evidence that suggests that either the cerebellum or MGN are involved in sleep regulation. Based on aspiration lesion data, Miller and colleagues suggested that the superior-colliculus-pretectum complex was involved in light-regulated REM-sleep episodes [25], but their more recent studies using more specific lesions demonstrated that it is the pretectum-geniculate complex that is important in this sleep regulation [26]. LGNd relay neurons are part of a glutamatergic corticothalamic feedback loop, which is hypothesized to have a critical role in the transition and maintenance of sleep stages [17–19]. Therefore, of the PLC-β4 immunoreactive brain areas, the LGNd is the most likely site of functional change underlying the irregular REM sleep observed in PLC-β4−/− mice.

Unusual body temperature rhythms were also observed in PLC-β4−/− mice (Fig. 2A). Body temperature rhythms in PLC-β4−/− mice displayed significantly smaller circadian amplitude with higher temperature levels during the daytime. This change in body temperature rhythms may not be due to the irregular set-point of thermoregulatory systems, since home-othermal responses against abrupt shift of ambient temperature levels were intact in PLC-β4−/− mice (Fig. 2B). It is rather conceivable that fragmentation of sleep episodes may be involved in this temperature elevation, since sleep durations are negatively correlated with body temperature levels in rodents [27]. In fact, ultradian rhythms in body temperature levels, which are generally coupled to short-term sleep-wake cycles [27], were almost absent in PLC-β4−/− mice (Fig. 2A). Recent immunohistochemical studies demonstrated that number of PLC-β4-immunoreactive cells displayed circadian rhythms in the suprachiasmatic nucleus, suggesting possible roles of PLC-β4 on circadian clock functions [28]. It has been shown that outputs from the SCN strongly influence REM sleep transitions [29,30]. Therefore, reduced circadian amplitudes in body temperature rhythms may also be related to the outputs of circadian oscillator and resultant changes in REM sleep architectures, although neither our present results (Fig. 2A) nor previous studies [22] observed irregular circadian clock works, regarding the synchronization to environmental light-dark cycles.

In general, to determine the precise site of gene knockout effects on behavioral phenotypes, conditional knockout techniques and/or rescue techniques will be required. However, since PLC-β4 immunoreactivities were concentrated within the specific brain areas, we further analyzed the function of the LGNd, where is the most likely site of functional change underlying the irregular sleep sequence in PLC-β4−/− mice. The LGNd contains neurons that express various metabotropic receptors that may be involved in regulating sleep episodes [18]. To determine the predominant type of metabotropic receptors coupled to PLC-β4 in the mouse LGNd, we used macroscopic fura-2 Ca^{2+} imaging techniques. We first examined effects of orexin-A and −B on intracellular Ca^{2+} levels in the LGNd but failed to observe these responses (Fig. 4A). These results are consistent with previous reports showing little orexin immunoreactive projections to the LGNd [11] and no effects of orexin-A or −B on action potentials recorded in LGNd neurons [10]. In contrast, both DHPG and 1S,3R-ACPD increased intracellular Ca^{2+} in the LGNd (Fig. 4B,C). This result is
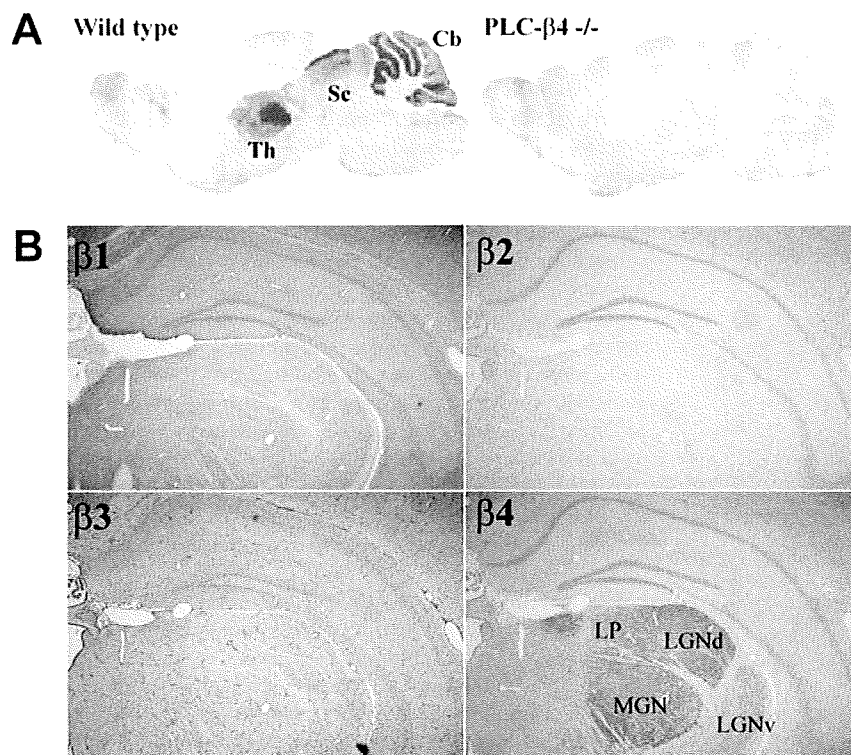
— 223 —

Figure 3. Localization of PLC-β families in the brain. A. Immunostaining with an anti-PLC-β4 antibody in sagittal brain sections from representative wild-type (left) and PLC-β4−/− (right) mice. Robust staining was observed in the thalamus (Th), superior colliculus (Sc), and cerebellum (Cb) in wild-type mice, but not in PLC-β4−/− mice. **B.** Immunostaining (orange-brown) of the thalamic geniculate nucleus and hippocampus of a wild-type mouse with PLC-β1-4 antibodies. No immunoreactivity was found for PLC-β2 and the section exhibits only cells counterstained with cresyl violet (blue). Robust immunoreactivity for PLC-β4 was observed in the medial geniculate nucleus (MGN) and the dorsal lateral geniculate nucleus (LGNd). The ventral lateral geniculate nucleus (LGNv) exhibited relatively less immunoreactivity. DG, dentate gyrus; CA3, CA3 region of the hippocampus; PT, pretectal nucleus.
doi:10.1371/journal.pone.0007737.g003

consistent with the dense mGluR1a immunoreactivity previously observed in the LGNd [31]. Since PLC-β4−/− significantly reduced DHPG-induced Ca^{2+} response in the LGNd, it seems likely that PLC-β4 couples primarily to group-1 mGluR in the LGNd. The LGNd also contains other mGluR subtypes, possibly group-2 (i.e., $G_{i/o}$-coupled inhibitory) mGluR [32]. Consistent with the presence of other mGluR subtypes, we observed a biphasic Ca^{2+} response followed by 1S,3R-ACPD stimulation and the negative phase was apparent when 1S,3R-ACPD was applied to the LGNd of PLC-β4−/− mice (Fig. 4B,C). Thus, the lack of PLC-β4 may result in a directional change in the response, from increasing Ca^{2+} to decreasing Ca^{2+}, with simultaneous stimulation of all mGluR subtypes in the LGNd.

It is notable that PLC-β4−/− did not completely abolish group-1 mGluR-mediated cellular response in the LGNd. Previous studies have shown that mGluR activation in the cerebellum of PLC-β4−/− mice resulted in a decrease of only 27% in total phosphoinositide hydrosis [33]. Single-cell-based analysis of Purkinje cells demonstrated no measurable group-1 mGluR responses in lobe 6, but intact responses in lobe 9 of the cerebellum of PLC-β4−/− mice [13,14], suggesting that there is heterogeneous expression of PLC subtypes in individual cells even within the same neuronal cluster. Also, group-1 mGluR are coupled to various intracellular signaling cascades, including PLC-independent cascades, such as G-protein activation of potassium channels in superior colliculus neurons [34]. Therefore, the residual Ca^{2+} response to group-1 mGluR activation in PLC-β4−/− mice observed in the present study may be explained by diversity in the

cell types in the LGNd and intracellular signaling mechanisms linked to group-1 mGluR.

In fact, our voltage-clamp recordings demonstrated that PLC-β4−/− had small effects on LGNd interneurons whereas the DHPG-induced current had a reversed polarity in LGNd relay neurons. This observation indicates that (i) group-1 mGluR were coupled to other PLC subtypes in LGNd interneurons, (ii) PLC-β4 was critical for normal group-1 mGluR signaling in LGNd relay neurons and there was no compensatory coupling to other PLC subtypes in these neurons and (iii) group-1 mGluR activated PLC-independent signaling pathways in the relay neurons of PLC-β4−/− mice, presumably via G-protein activation of potassium channels [34], which, in wild-type mice was usually masked by phosphatidyl inositol cascades. Thus, disrupted group-1 mGluR signaling in LGNd relay neurons likely underlies the irregular sleep sequences in PLC-β4−/− mice, although further studies will be required to prove this hypothesis.

The molecular mechanisms and critical neuronal networks underlying REM sleep switching remain unclear. For example, gene-knockout mice lacking serotonin 1B receptors [35], norepinephrine [36,37], or histidine decarboxylase (i.e., the histamine synthetic enzyme) [38] have been used to investigate REM sleep, but these knockout animals exhibit only a partial decrease or increase in REM sleep, and the phenotype is less dramatic than that of orexin-deficient or PLC-β4−/− mice. It is also unclear if the disruption of REM sleep in serotonin-, norepinephrine-, or histamine-deficient animals involves any changes in the hypothesized REM-sleep-regulating networks, because these receptors
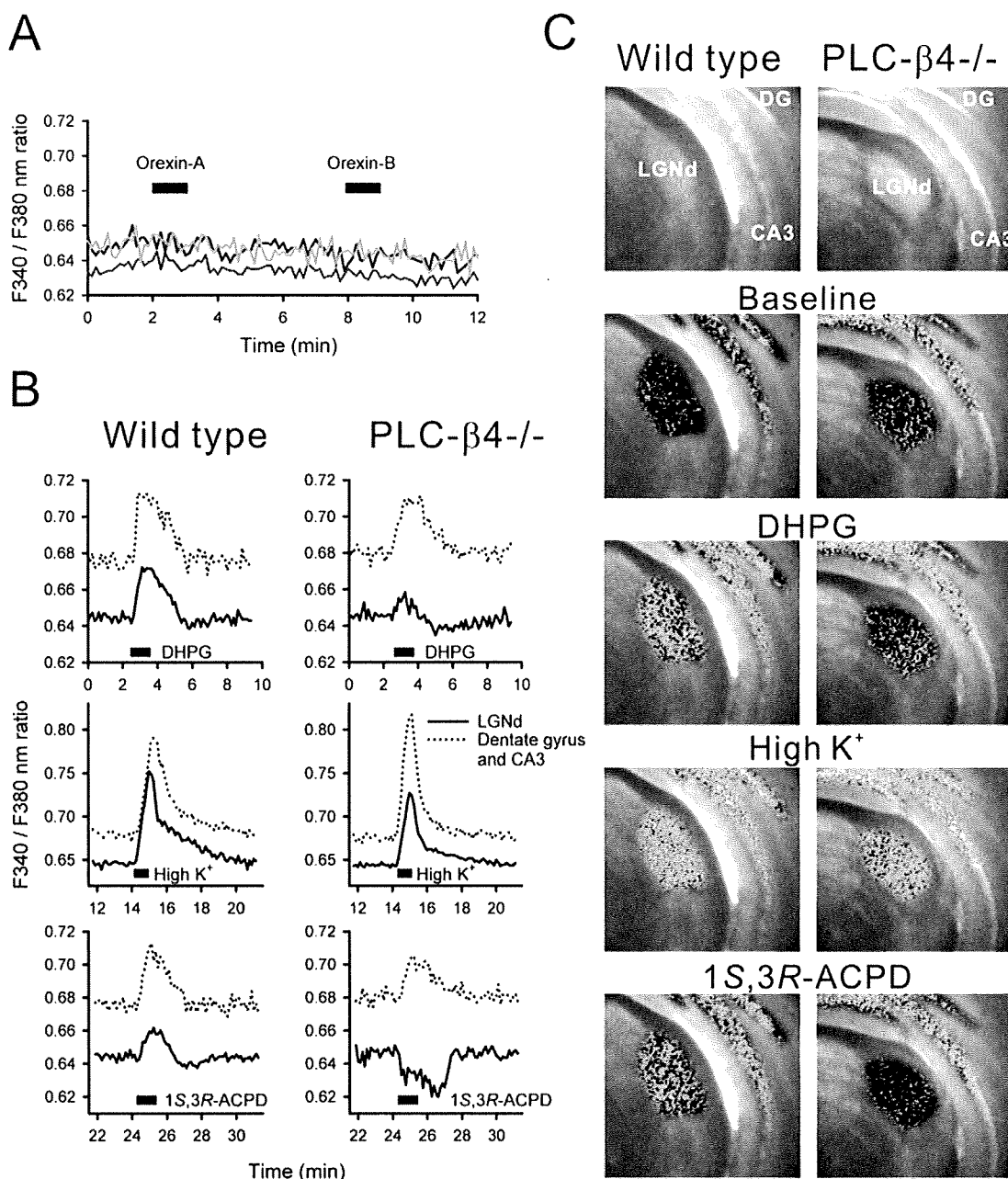
Figure 4. The metabotropic receptors linked to PLC-β4 in the LGNd were analyzed using Ca²⁺ imaging techniques. A. Orexin-A (300 nM) and orexin-B (300 nM) failed to mobilize intracellular Ca²⁺ in the LGNd of wild-type mice. Intracellular Ca²⁺ levels in LGNd from 3 different animals were plotted in this graph. **B.** The group-1 mGluR agonist, DHPG (100 µM), and the nonspecific mGluR agonist, 1S,3R-ACPD (100 µM), induced increased the intracellular Ca2+ in the LGNd (solid lines) of wild-type mice (left column). In PLC-β4−/− mice (right column), DHPG induced a significantly smaller Ca²⁺ increase while 1S,3R-ACPD decreased in Ca²⁺ in the LGNd. Control responses to 50 mM high-K⁺ stimulation (middle row) and in the dentate gyrus/CA3 region of hippocampus (broken lines) are also shown. **C.** Corresponding virtual color images of intracellular Ca²⁺ levels in the LGNd (approximate area is outlined in red in the top images) and dentate gyrus (DG)/CA3 region of the hippocampus were superimposed onto the transmitted light images shown at the top. Increasingly warmer colors indicate higher Ca²⁺ levels. Baseline was taken from the first frame of experiments. Frames of DHPG, high K⁺, and 1S,3R-ACPD were obtained from the peak Ca²⁺ response times in the dentate gyrus/CA3 region. All experiments were conducted in the presence of 1 µM tetrodotoxin.
doi:10.1371/journal.pone.0007737.g004

and substances are widely distributed throughout the brain, as in the case of orexin-positive fibers.

Tonegawa's group used the gene promoter sequence for the K$_v$3.2 potassium channel to enable conditional knockout of T-type Ca²⁺ channels (Ca$_v$3.1) in the rostral-midline thalamus, and observed frequent transitions between non-REM sleep and wakefulness [39]. Several nuclei in the rostral-midline thalamus

have been shown to contain orexin-receptive neurons [9,10]. Although REM sleep is intact in Ca$_v$3.1 knockout mice, it is a reasonable hypothesis that heterogeneous neuronal clusters in the thalamus have a critical role in the regulation of sleep-wake transitions. The rostral-midline thalamus is near to but apparently separate from the PLC-β4-positive thalamic nuclei. Since the present study did not find direct molecular communications

— 225 —